QATAR UNIVERSITY

COLLEGE OF ARTS AND SCIENCES

# PREPARATION AND CHARACTERIZATION OF NANOSTRUCTURE MATERIAL FOR BIOLOGICAL APPLICATION

BY

WIDAD MOHAMMED H. Q. ALKHULAQI

A Thesis Submitted to

the College of Arts and Sciences

in Partial Fulfillment of the Requirements for the Degree of

Masters of Science in Material Science and Technology

January 2023

# COMMITTEE PAGE

The members of the Committee approve the Thesis of
Widad Alkhulaqi defended on 12/01/2023.

Prof. Ahmed Elzatahry
Thesis/Dissertation Supervisor

Prof. Khaled Saoud
Co-supervisor

Prof. Gheyath Naserallah
Committee Member

Approved:

Ahmed Elzatahry, Dean, College of Arts and Sciences

# ABSTRACT

ALKHULAQI, WIDAD, MOHAMMED. Masters: January: [2023:] Material Science and Technology

Title:_Preparation and Characterization of Nanostructures Materials for Biological Application.

Supervisor of Thesis: Ahmed Elzatahry

Currently, nanomaterial has gained much attention in medical applications. Two different nanostructured materials were synthesized for biomedical purposes in this approach. Firstly, a composite of bimetallic nanoparticles containing Ag and Ni supported on metal oxide ($TiO_2$) was successfully fabricated by co-precipitation manner via $NaBH_4$ as a strong reducing agent employed as a photocatalyst and disinfector. A 1 g/L of NiO/Ag/$TiO_2$ nanocomposite was assessed towards the decomposition of dyes (Methylene blue (MB)), Aspirin, and Paracetamol as pharmaceutical waste with a reduction rate of (93.19%, 77%, and 68.4%, respectively) under visible light within 60 minutes. Furthermore, the effect of annealing was studied which represents a faster degradation of MB dye and higher efficiency reaching 95.92% under visible light within 60 minutes. The basic mechanism of the photodegradation of MB via NiO/Ag/$TiO_2$ nanocomposite was outlined. In addition, even after three cycles, the catalyst showed a significant degrading efficiency reached 90.4%. Next, the nanoparticle was evaluated against two different strains of bacteria (E. coli and Staphylococcus aureus.) in both visible light and dark conditions. The composite shows a dose-dependent bacteriostatic in both bacteria and has a bactericidal effect on E. coli that are exposed to 1 g/L of the material. Second, the preparation of virus-like silica mesoporous nanoparticles (V-MSN) as a drug carrier was done in this work. Due to their biomedical application, it is essential to find the in-vivo model toxicity of this medical carrier. However, the drug has been found to be non-hazard for doses up to 1000 mg/L tested on the zebrafish

embryos model.

# DEDICATION

*First of all, I dedicate this thesis to Allah, thanks for guiding me, giving me healthy life and protecting me, and to the prophet Muhammad for inspiring me.*

*To my family for their unlimited support and patience.*

# ACKNOWLEDGMENTS

I would like to acknowledge the support of Qatar University for providing all the needs to achieve the requirements of this study.

First, I would like to sincerely thank, appreciate, and acknowledge my supervisors, Dr. Ahmed Elzatahry for his support and gave me the fantastic opportunity to work on my thesis under his guidance. To Dr. Khaled Saoud from Virginia Commonwealth University (VCU), who is the main responsible for my success in this thesis, for his help and constant feedback and pieces of advice. To Dr. Gheyath Nasrallah from the biomedical center research (BCR) at Qatar University. Many thanks for giving me the chance to work in his lab with his cooperative team and for the advice given.

I would like to thank all faculty members of the material science and technology program: Dr. Khaled M. Youssef, Dr. Talal M. Al-Tahtamouni, and Dr. Ahmed Elzatahry, and from the center of advanced material (CAM): Dr. Mohammed Hassan and Dr. Igor Krupa for giving us valuable courses and for their effort and support since the beginning of this program.

Special thanks to VCU members especially to Mrs. Maha Almatalkah for sharing her knowledge, assistance and helpful instruction, and to Dr. Ahmed Sarraj from Hamad bin Khalifa University. Moreover, it is my pleasure to work with Dr. Gheyath's team especially, Ms. Farah, Ms. Inas, and Mrs. Nadine. I appreciate all your kind help, your time, guidance, and patience. I am thankful to Dr. Ahmed Elzatahry's research team, especially Mr. Yaseen Ibrahim, Mr. Abdulla Alashraf from CAM, and Mr. Asem Taha from the Chemistry and Earth Department for their help. Also, I acknowledge the Qatar University Central Laboratories unit (UCL) for their assistance in the characterization.

In addition, I would like to acknowledge Qatar National Research Fund (QNRF) for their financial support project no. [NPRP12S-0309-190268], Virginia Commonwealth University in Qatar (VCU Art Qatar) /Qatar Foundation-Nanotechnology and Textile Research Lab fund grant number [HQ1240] for their support and the Qatar National Library for providing open Access funding.

# TABLE OF CONTENT

# LIST OF TABLES

# LIST OF FIGURES

# CHAPTER 1: INTRODUCTION

Nanomaterials are being used in a variety of industries, including the food industry, medicine, and the environment[1]–[4]. The latest developments have improved the modeling and designing of various biological and medical equipment and applications [5]. Nanomaterials' distinctive qualities are a result of their small size (1–100 nm). They have high surface areas, strong mechanical and thermal stability, high electrical characteristics, high optical and magnetic characteristics, and large surface areas. Due to their distinctive physical and chemical characteristics, nanoparticles (NPs) are gaining huge interest as potential biological materials, and research into them is expanding[6]. These NPs can be made of a wide range of substances, such as noble metals (such as Au, Ag, Pt, and Pd), semiconductors (such as CdSe, CdS, ZnS, $TiO_2$, PbS, InP, and Si), magnetic compounds (such as $Fe_3O_4$, Co, $CoFe_2O_4$, Fe) and other core-shell NPs and other composite nanostructures such as homogeneous and heterogeneous composites)[6]–[10]. These nanostructures can employ as a catalyst, drug carriers, sensors, disinfectors, water splitting, energy storage, etc.[11]–[16].

The design and fabrication of functional nanoparticles for biological applications can prevent the spread many of diseases. Due to the recent spread of many intestinal diseases, heterogeneous photocatalysts will prepare to prevent the proliferation of microbes and reduce water contamination. Recently, the excellent and wide photocatalytic activity of nanocomposite heterogeneous photo-catalysts resulting from interactions of light with scattered nanomaterials has attracted concerns. Titanium dioxide ($TiO_2$) due to the chemical stability and the good reactivity under UV irradiation (k 390 nm) has gained a lot of interest among many metal-oxide compounds getting designed for photocatalytic degradation [17]. There are many studies that reported the effect of $TiO_2$ in inhibition of the bacteria, molds, viruses, and cancer cells [17]. However, because the $TiO_2$ has a large band gap (3.2 eV), it only can be useful under the UV radiation of the spectral region (5 % of solar energy), whereas

visible light includes roughly 45% [17]. Metallic doping has increasingly been known as among the most successful methods for modifying $TiO_2$'s intrinsic bandgap which leads to improving its visible light absorbance and photocatalytic activity. Ag metals have gained a lot of attention as dopants for this aim. However, Ag has long been recognized as among the most intriguing antibacterial agents. Ag+ is thought to connect to the slightly negative microbial cell wall membrane, degrade it, and therefore influence its performance Ag+ can bind with thiol groups in proteins, inactivating respiratory enzymes and allowing the production of reactive oxygen species.[17], [18] As previously stated, silver particles allow $TiO_2$ to be excited by visible light. It is discovered that Ag doped in $TiO_2$ significantly increased photocatalytic bacterial inhibition. For example, adding 1 wt% Ag to $TiO_2$ lowered the reaction time necessary to fully remove 107 CFU/mL of E. coli by 65 to 16 minutes under UV radiation. That happens by decreasing the recombination rate of the $TiO_2$ by Ag nanoparticles of it is electron-hole peer charge carriers and increasing the surface area for adsorption. [17] Furthermore, other research approved those bimetallic composite nanoparticles, which are made of two various metal elements, are more interesting than monometallic nanoparticles because they may have special electronic, optical, catalytic, or photocatalytic characteristics that do not appear when using monometallic nanoparticles [19]. Verbruggen et al. claims that the Au-Ag alloy on $TiO_2$ photocatalysts has activity within the visible light range.[20]

Besides, for other bio applications, they found that viruses show good cellular infestation because of their rough surface that contains of spike proteins which have a significant ability to attach to the cell wall during the infestation process.[21] Several kinds of research have been applied to synthesize nanoparticles with the topological structures of viruses, influenced by the distinctive surface roughness of viruses[22]. However, their time-consuming and uncontrolled manufacturing procedures and also their poor permeability and

aggregation, severely limit their potential uses in biomedicine, including such intracellular delivery of drugs. To fit the criteria of efficient cellular reception for diverse biological purposes, constructing well-controlled virus-like nanostructures with superior dispersibility and creating large channels will get a lot of attention.[23] One paper indicates a novel manner to synthesize virus-like mesopores silica which has a hollow nanosphere surrounded by vertical epitaxial hollow nanotubes.[24] Hence, the synthesis of virus-like mesoporous silica nanoparticles can enhance cellular internalization indicating valued drug delivery ability as well as minimize the toxicity toward other healthy organs.[24]

This thesis will focus on preparing and characterizing heterogeneous catalysts (bimetallic supported on $TiO_2$), testing the photocatalytic activity against dyes and organic pollutants, and using it as an antibacterial in light and dark conditions. Second, synthesizing a virus shape of mesoporous silica nanoparticles and testing the cytotoxicity by using an in-vivo model (zebrafish embryos).

# CHAPTER 2: A LITERATURE REVIEW OF THE CATALYSTS AND THEIR APPLICATION

## 2.1 History of Catalysis

Since the dawn of humankind, fermenting has been used to create alcohol from sugar. In 1552, Valerius Cordus (1514–1554) employed sulfuric acid to accelerate the conversion of alcohol to ether, marking the first recorded use of inorganic catalysts. When potato starch, distilled water, and cream of tartar (potassium hydrogen tartrate) were combined, Antoine Augustin Parmentier (1737–1813) discovered in 1781 that after many months, the mixture develops a pleasant taste that is more prominent when acetic acid is used. Johann Wolfgang Döbereiner (1780–1849) conducted a more extensive investigation of this process and discovered that starch dissolved in water ferments into alcohol; he assumed that the starch was firstly turned into sugar. Additionally, he observed that manganese dioxide catalyzed the thermal breakdown of potassium chlorate, the precursor of oxygen. Thenard linked the behavior of yeast during the fermentation process to the impact of uniformly divided metal on hydrogen peroxide in 1820. Thenard's description of the fermentation mechanism is cited by Louis Pasteur (1822–1895) in his popular study of alcoholic production [25].

Peregrine Phillips, who had previously achieved an English patent to produce sulfuric acid in 1831, participated in the commercial uses of Döbereiner's finding that sulfur dioxide can be oxidized by the atmosphere to sulfur trioxide in the availability of platinum in 1832. A method for producing sulfuric acid by oxidizing sulfur on finely fragmented platinum supported on a glass or another acid-resistant material was patented by Kuhlmann in 1838.[26]

The first person to investigate the inactivation of platinum-based catalysts was William Henry (1774–1836). Henry found that some compounds, such as carbon disulfide and hydrogen sulfide prevent the combustion of hydrogen and that platinum catalysts are less

effective at igniting the combustion of methane and ethylene than they are at igniting the combustion of hydrogen and carbon monoxide. Following Döbereiner, he employed platinum sponge or platinum-clay balls as a catalyst. These significant breakthroughs in the development of catalysis inspire several other studies and advancements.[26], [27]

## 2.2 Types of Catalysis

### *2.2.1 Enzymatic Catalysis*

Enzymes are catalysts that can be derived from biological organisms and are used to speed up chemical reactions without being consumed. [28], [29] In the live cells, these catalysts either start or influence nearly any biochemical process. [28], [29] Distinct three-dimensional structures that match the geometry of the reagents are present in each enzyme[28], [29]. Currently, the role of biocatalysts in the investigation of biodiesel production has become increasingly important. [30] It is thought that these catalysts will outperform synthetic catalysts. [30] The use of proteins as catalysts was investigated in the research for an environmentally safe technique for producing biodiesel. [30] Enzyme-catalyzed transesterification procedures generally solve challenges faced by traditional catalysts, such as employed feedstock pretreatment, catalyst removal, effluent treatment, and high-energy need. [30] Employing an accumulation of lipases produced by microbes, animals, and 883 plants, biocatalysis is carried out[30]. Lipases can be isolated from a variety of species of bacteria, including Candida rugosa, Thermomyces lanuginosus, Pseudomonas fluorescens, Pseudomonas cepacia, Rhizomucor miehei, and Rhizopus oryzae[31].

Biocatalysts can be divided into the following main categories. (a) Microbes: An organism that is tiny in size, including yeast and other anaerobic bacteria, Archaea, bacteria, fungus, viruses, and microbial mergers. (a) Lipases: The most popular category of enzymes for organic synthesis, 889 lipases are recommended because they are more stable than other biocatalysts. Extracellular and intracellular lipase are two different types of lipases[31]. Extracellular lipases are primarily isolated via purifying from live-producing microbe broth.

R. oryzae, C. Antarctica, P. cepacia, and Mucor miehei are the main extracellular microbes. The cell-producing membrane or its inner include intracellular lipases. [31] Intracellular lipases are typically observed immobilized. Proteases are enzymes that digest proteins. [31] Animals, plants, bacteria, archaea, and viruses all have this class of proteases. TEV protease and trypsinogen, as examples. Cellulases are the enzymes that degrade cellulose. The enzymes known as amylases convert starch into simple sugars.[31]

### *2.2.2 Homogeneous Catalysis*

In homogeneous catalysis, a catalyst from the identical phase as the reagents is used in a series of reactions. [32] Solid, liquid, and gas phases are all used. In most cases, a homogeneous catalyst is co-dissolved in the solvent together with all the reagents. [32] There are several significant benefits that homogeneous catalysts have over their heterogeneous counterparts. [32] For instance, since this catalyst is often a dissolved metal complex, all catalytic regions are accessible. Additionally, it is frequently able to modify the catalyst's chemo selectivity, regioselectivity, and/or enantioselectivity. [32] Considering these benefits, a significant drawback of homogeneous catalysts over heterogeneous catalysts has prevented the widespread commercialization of several homogeneous catalytic systems: the challenge of separating the reaction product from the catalyst and from any reaction fluid. [32] This issue arises since distillation, the most popular separating technique, needs high temperatures unless the product is extremely volatile. [32] Most of the homogeneous catalysts are thermally delicate and typically break down below 150°C. [32] The frequently pricey catalyst will therefore disintegrate due to the heat stress brought on the product distillation, even at low pressure. [32] Catalyst degradation can also result from other traditional procedures like chromatography or extraction. [32] The homogeneous processes that have been commercialized either use volatile products and substrates or don't have any organic ligands that are heat-sensitive [32].

### *2.2.3 Heterogeneous Catalysis*

In chemical science, heterogeneous catalysts are essential for many chemical reactions. The catalytic reaction results in the formation of new chemical bonds as well as the breaking of existing ones. [33], [34] These reactions keep happening, mainly without a dramatic change in the catalyst. However, this chemical transformation would either not happen or would happen more slowly or with poorer efficiency without the presence of the catalyst.[33], [34] One of the more appealing aspects of the heterogeneous catalytic system is the separation, purification, and reuse of the catalyst. Zeolites and inorganic oxides are crucial components of heterogeneous catalysis[32].

## 2.3 Nanoparticles Catalysts

Microorganisms are common in water and on surfaces, and medicines, phenolic compounds, and pigments have all been found in water sources recently[35]. The most dangerous pollutants on the water's surface and bottom are thought to be pharmaceutical waste and dyes like Methylene blue (MB). Designing light-driven water contamination removal materials that are efficient, doable, and visible is crucial for practical utilization. In this study, a high-efficiency green photocatalytic ternary nanocomposite is proposed and created for the treatment of water pollution[36].

The use of photocatalysts in medicine and the environment has generated a lot of interest recently. [37] $TiO_2$ shows great promise as a photocatalyst for the removal of pollutants and pathogens under varied irradiation circumstances. [37] Photocatalysts made of heterogeneous metal and metal oxide semiconductors are extensively utilized to reduce water and air pollution. [37] When exposed to ultraviolet (UV) radiation, they also demonstrate notable effectiveness in eliminating organic pollutant dyes, pesticides, and pharmaceuticals.[37].

For photocatalytic activity to occur, the catalyst must be able to produce electron-hole pairs. [38] Because of this behavior, free radicals ($OH^{\bullet}$) are created, which could lead to other

reactions. [38] Organic compounds, including harmful chemicals, germs, and viruses, can be successfully broken down into $CO_2$ and $H_2O$ using photocatalysis using semiconducting nanoparticles. [38] Metal oxides, such as $TiO_2$, ZnO, CuO, and $WO_3$ nanoparticles, have been utilized extensively for destroying bacteria, viruses, and hazardous contaminants in presence of UV irradiation. [38] $TiO_2$ is a well-known photocatalytic chemical with a long history of commercial application. Despite being inexpensive, stable, and corrosion-resistant, $TiO_2$ has a broad bandgap energy of 3.2 eV, necessitating intense UV irradiation for activation. [38] It is possible to enhance the use of solar light for a photocatalytic or photo-electrochemical process by shifting the bandgap of $TiO_2$ to the visible or infrared range. [38] Additionally, common homogeneous photocatalysts based on $TiO_2$ have inherent limitations such as rapid electron-hole pair recombination.[38] However, based on the alteration of the bandgap and increase in charge carrier separation, heterogeneous photocatalysis has proven to be more fascinating than its homogeneous counterpart[38].

## 2.4 Preparation of Supported Metal Nanoparticles Catalysts

The adjustment of physiochemical characteristics (size, morphology, and composition) is crucial for the nano-catalyst. It will be immensely beneficial for photocatalytic activity and other applications. Therefore, we must have techniques used for creating photocatalysts using desirable characteristics. Additionally, catalyst synthesizing should be economical and eco-friendly. There are several methods for catalyst manufacturing which are discussed below. [38]

### *2.4.1 Sol-gel Method*

In the heterogeneous sol-gel approach, the active component's porous precursor is impregnated with the textural promoter precursor in a quantity anticipated to have a specific weight ratio between the active component and textural promoter in the finished product. [38] The purpose of the textural promoter is to maintain the structure of the active component and

stop it from sintering during posttreatment. As textural enhancers, difficult-to-minimize oxides (HRO) like silica or alumina are typically used. You can combine ingredients such as tetraethoxysilane (a precursor to a textural enhancer) with ethanol, iron nitrate (a precursor to the active component), and silica to create iron/silica nanocomposite particles. After drying to eliminate the excess water and solvent, the mixture is then gelled before being calcined[39].

### *2.4.2 Chemical Vapor Deposition (CVD)*

One of the most widely utilized for the deposition of nanomaterials as a thin film is the CVD technique.[40] Typically, these procedures are employed to create thin films on surfaces of substances to modify the mechanical, electrical, thermal, optical, wear-resistant, and anticorrosive capabilities of diverse substrates. [40] The vapors in the CVD chamber are heated using thermal energy, which also initiates the coating reaction. [40] Numerous variables influence the development of CVD. [40] There are significant parameters that can impact the CVD mechanism such as deposition chamber geometry, gas composition, flow rate, deposition temperature, and pressure. These are the variables that aid in controlling the target structure's nanoforms. [40] The size and dispersion of the nanograins in the layers are influenced by the substrates, according to Djerdja et al., who reported nanocrystalline $TiO_2$ films produced by CVD on several substrates at a low temperature of 320°C employing titanium tetrachloride as a precursor[41]. The second CVD method uses a substrate for CVD deposition that has been prepared using a template. [42] For instance, they've utilized a CVD using concentric $TiS_2$ exterior nanotubules to cover a group of gold nanotubules. The electroless deposition of gold tubules or fibrils into the membrane pores of a template is required as the initial stage in this procedure. [42] One side of the plated wall has its Au surface layer eliminated, and the membrane is then disintegrated.[42]

### *2.4.3 Hydrothermal Method*

The hydrothermal process is often carried out in steel autoclaves at regulated temperature or pressure with the reaction taking place in aqueous systems. [39] When the reaction temperature is raised beyond the boiling point of water, the pressure of vapor saturation is reached. [39] The autoclave's temperature and the volume of solution supplied are the main determinants of the inner pressure generated. [39] The hydrothermal approach is described as any heterogeneous process taking place under extreme pressure and temperature settings in the presence of aqueous solvents or mineralizers to dissolve and recrystallize materials that are relatively insoluble under normal circumstances. [39] The solvent is employed in this procedure at extreme temps (often between 100°C and 1000°C) and high pressures (typically between 1 atm and 10,000 atm), which promotes precursor contact throughout production. [39] The process is known as hydrothermal synthesizing if water is utilized as the solvent[39].

### *2.4.4 Coprecipitation Method*

Co-precipitation is the method used most frequently to make mixed-oxide catalysts. [39] It provides for the simultaneous precipitation of the metal and the support material using an aqueous alkali (such as NaOH, $Na_2CO_3$, or $K_2CO_3$). This method generally makes it possible for the metal and the supporting medium to react strongly. [39] Deposition precipitation, a related but different method, needs the metal precursor to being added to an aqueous suspension of the support medium before the hydroxide is precipitated off by raising the pH. The support particles' surfaces operate as nucleating agents to strengthen the link between the active precursor and the support. [39] The necessary end chemical can subsequently be created by calcining and reducing the resultant hydroxide species[39].

## 2.5 Water Treatment Application

The perfect adsorbent for wastewater treatment is nanostructures particles, which may be used in a variety of ways, including as a catalytic, absorptive, catalytic membrane,

bioactive nanoparticles, biomimetic membrane, polymeric and nanocomposite membrane, and thin film composite membrane. However, it has been observed there is effectiveness in dye removal, degradation of pharmaceutical and organic wastes, and anti-bacterial activities. [43], [44]

### *2.5.1 Removals of Dyes*

Manufactured dyes are essential in several key businesses, including the leather, paper, and textile sectors, due to their ability to produce color. According to estimates, 700 000 tones of varied colors are produced a year from 100, 000 commercially available dyes. After pigments have completed their intended function, most of them are frequently dumped carelessly into environmental water sources[43], [44].

Dye effluents also referred to as dye wastewater, are highly concentrated in dangerous compounds. Because dye effluents are poisonous by nature, they could damage both human and animal life. [45] These days, removing dye molecules from water sources is not only difficult but also a significant environmental concern. Recent focus has been given to methods of treating and recycling dye effluent because, absent a reliable solution, pure water sources may soon start to quickly diminish. The environment would substantially advantage from the development of a fixed solution to permanently remove pigment particles from textile effluents.[45]

Scientists now have renewed optimism in finding a cure for cancer-causing dyes because of nanotechnology. [36] It is necessary to remove toxins from water sources, such as dyes, by nanoparticles like zinc oxide, titanium, iron oxide, and silver having photocatalytic performance, antimicrobial activities, and rapid oxidation, making them excellent for treating pigments found in water.[36] Because of the distinct physiochemical features of nanoparticles, the quickly developing field of nanotechnology has demonstrated potential for treating effluent over time.[36]

Nanoparticles are effective adsorbents due to their high surface area to volume ratio, low diffusion resistance, quick adsorption equilibrium, and increased adsorption capacity. [36] When adsorbing onto nano-silica powder made using silver nanoparticles, dyes such as Eosin yellow, Congo red, brilliant blue, and Bromophenol blue showed 99% dye removal at an initial concentration of 50 mg/L. An 86% dye desorption rate observed during acetone-based desorption experiments prompted additional exploration into the recyclability of new adsorbents. [36] Furthermore, magnetic nanoparticles have also been extensively used since they are simple to separate using an outside magnetic field[36].

According to reports, chitosan-encapsulated zinc oxide (ZnO) hybrid composites have excellent photocatalytic properties towards the dye methylene blue when exposed to UV light, and 64% of the dye will be destroyed in 3 hours[46]. In addition, Solar-powered photocatalysis utilizing titanium dioxide ($TiO_2$) has become a potential strategy for addressing environmental problems. [38] It has been discovered that anatase $TiO_2$ and N-doped $TiO_2$ exhibit strong photocatalytic activity when exposed to both UV and visible light. The photocatalytic activity begins with the absorption of photons. [38] When the band gap of $TiO_2$ is stimulated, conduction band electrons (cb(e-)) and valence band holes (vb(h+)), also known as electron-hole pairs, are produced. [38] These charge bearers may recombine again without generating heat, or they could go to the surface, where they might become trapped and ultimately react with the right electron donors and acceptors to create reactive oxygen species (ROS). [38]

### *2.5.2 Reduction of Pharmaceutical Compounds Residues.*

Pharmaceutical residues have been found to significantly adsorb into the soil as toxicants, making complete removal from wastewater and activated sludges difficult.[47] The advanced oxidation process (AOP) is very effective in treating this situation because it involves the production of highly reactive hydroxyl radicals that oxidize the

micropollutants.[48] AOPs are chemical remediation procedures that decompose and eliminate organic pollutants using reactive oxygen species (ROS).[48] According to Kaushik et al. (2019), “Titanium oxide's adsorption behavior against contaminants also enhances synergistically in visible light, resulting in its strong photocatalytic activity.” [49] This is because nanoparticles have a large surface area. [49] Regarding studies, “One of the best effective photocatalysts for the breakdown of various antibiotics, including fluoroquinolones, tetracycline, lincomycin, and oxolinic acid, is titanium dioxide (TiO2).” Sulfamethazine (SMT) was photo-catalytically degraded on $TiO_2$/CuxO nanotubes (NTs) under low-intensity solar light and indoor visible light irradiation. This process was examined, and SMT degradation was completed in the presence of $TiO_2$/CuxO nanotubes (in acid aqueous solution) in 3 hours. Likewise, ZnO/CuxO hexagonal nanowires were used to study the photocatalytic destruction of SMT. AgxO/FeOx/ZnO nanotubes (NTs), in which Ag doping considerably enhanced ZnO absorption in the visible region, have reported the breakdown of tetracycline (an antibiotic). Ag, which serves as a trapping site for the charges generated on ZnO by light, hinders charge recombination, while FeOx makes ZnO's response more visible. [50] However, Aspirin and Paracetamol are also reported as water pollutants. Previous work proved that $TiO_2$ has the efficiency to break down the aspirin molecule by doping with Fe. The results represented that aspirin was eliminated up to 96% by 0.5% Fe–$TiO_2$ under solar irradiations within 6 hours.[50] Furthermore, the analysis indicates that 66% of the paracetamol had been oxidized after 90 minutes of visible light irradiation in the presence of 50% $TiO_2$/$Fe_2O_3$. [51]

### *2.5.3 Killing and Inhibiting Bacteria*

Nanotechnology provides an opportunity to reexamine the biological characteristics of previously established antibacterial substances by adjusting the particle size from the bulk to the nanoscale which leads to a change in its effect. Long recognized for its antibacterial

activities, silver's use in medicine decreased with the advent of antibiotics.[52] According to numerous research, “Silver NPs have greater antibacterial activity than silver ions.” [53]–[55]Based on a recent paper, the regulated release of the silver ions causes carbon nano scrolls containing silver nanoparticles to have longer-lasting antifungal effects.[56] Owing to its potential cytotoxicity, regulatory institutions have recently expressed less interest in nano-Ag. have also demonstrated the potent antibacterial action of various metals, including gold, metal fluorides, and metal oxide nanoparticles, against a variety of pathogenic microbes. [57]Also recently reported was the sonochemical production of a Zn-doped CuO composite (i.e., ZnCuO), which showed better antibacterial capabilities than those shown with CuO or ZnO NPs alone. [57]Another example is carbon nanotubes since single-walled carbon nanotubes with high levels of purification have also been found to have potent antibacterial properties. [58] Also, $TiO_2$ nanoparticles have been reported that can work as bacteria deactivation. [59] The photocatalytic process begins with the absorption of light. When the band gap of $TiO_2$ is stimulated, conduction band electrons (cb(e-)) and valence band holes (vb(h+)), also known as electron-hole pairs, are produced. [59] These charge carriers may combine again without generating heat, or they could go to the surface, where they might become trapped and eventually react with the right electron donors and acceptors to create reactive oxygen species (ROS). [59] The bacterial cell wall may then be attacked by the reactive oxygen species (ROS), leading to cell death as represented in Figure 1. However, $TiO_2$ nanoparticles showed less toxicity than other nanostructured materials. [59]

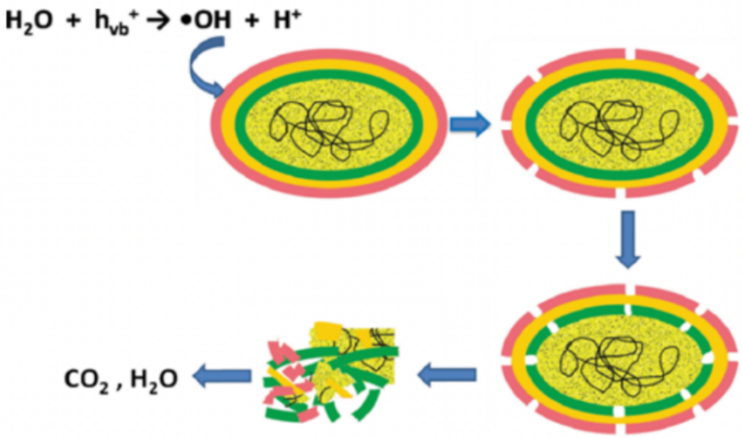


Figure 1. Mechanism of bacteria inhibition by radicles produced from nanoparticles.

Moreover, the bacterial cell wall's structure has a significant impact on the photocatalytic antibacterial activity of $TiO_2$. Even though several investigations on numerous species have been conducted, the findings are rather inconsistent. According to certain scientists, "Gram-positive bacteria is reportedly more susceptible to photocatalysts than Gram-negative bacteria." Although a lot of research has shown that Gram-negative bacteria is more resistant to photocatalytic bactericidal activity than Gram-positive bacteria. It is nevertheless important to note that this is true. Due to the nature of their cell wall, which limits the absorption of many chemicals to movements through the cell membrane, gram-negative bacteria are considerably more immune. The variation in cell membrane composition between Gram-negative and Gram-positive bacteria is often blamed for the variation in the photocatalytic inactivation of bacteria (Figure 2). Gram-negative bacteria have a triple-layered cell wall made up of an inner membrane, a thin coating of peptidoglycan, and an outside membrane, while Gram-positive bacteria only have a thicker layer of peptidoglycan. This also causes the various sensitivities of bacteria's cell walls and photocatalysts. This study will apply strategies to enhance the photocatalytic activity as well as the anti-bacterial properties of $TiO_2$[60]–[63].

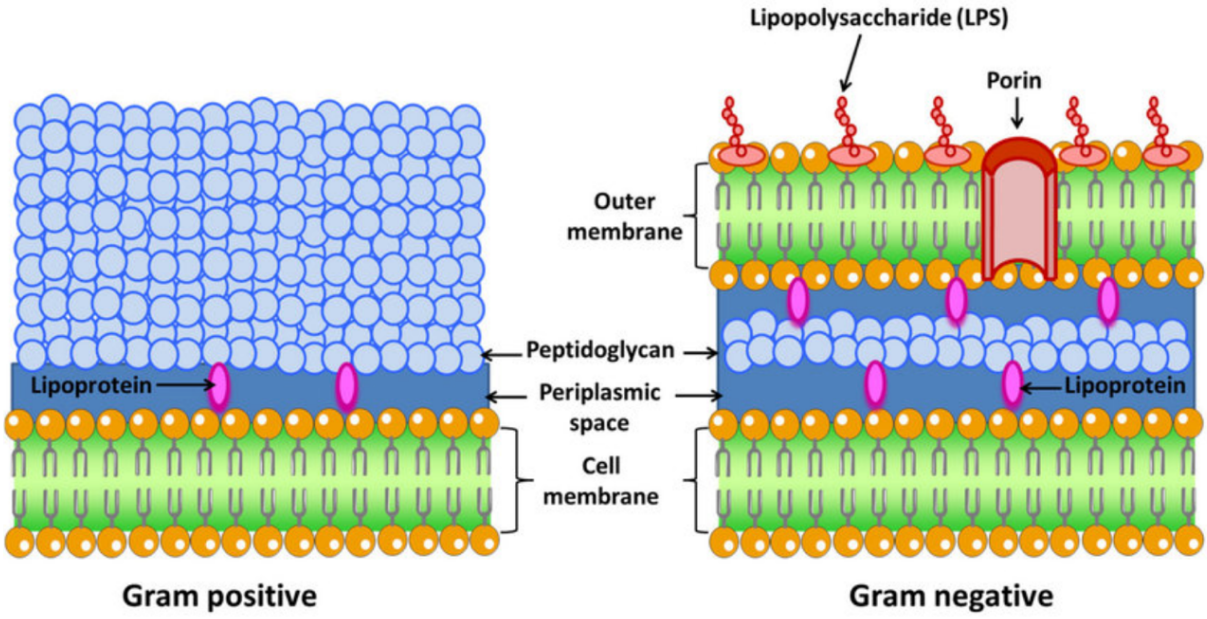


Figure 2. Differences between gram-positive and gram-negative membranes of bacteria.

## 2.6 Strategies for Enhancing the Photocatalytic Activity of $TiO_2$

Various strategies have been used to increase $TiO_2$ photocatalytic efficiency. In the literature on $TiO_2$ optimization, there are conflicting data. [64] This is probably because altering composition or morphology always changes other factors that have an impact on performance. [64] The recombination of photogenerated charge carriers, which diminishes activity, is the main flaw in semiconductor photocatalysis. Numerous methods have been used to boost photocatalytic activity, namely heterojunction coupling, doping with metals and non-metals, and modifying the optical characteristics of $TiO_2$ by narrowing its electronic properties. [64] Doping $TiO_2$ with transition metal ions is one of the most effective methods for producing a visible-light-driven photocatalyst and delaying potential electron-hole recombination. [64] The broadband gap of $TiO_2$ photocatalyst, which is in the UV spectrum region, limits its possible applications[64].

### *2.6.1 Metal Doping*

Within the band gap of a semiconductor, transition metal ions can offer further energy

levels. [65] Lower photon energy is needed for electron transport from one of these levels to the conduction band than it would be for a semiconductor without modifications. [65] For visible light photocatalytic activity, $TiO_2$ has been doped with a wide variety of transition metals, however, there are very few studies on visible light antibacterial activity. [65] $TiO_2$ metal doping has been thoroughly investigated as a method to enhance photoactivity under visible light irradiation[65].

Numerous research has documented the synthesis of copper-modified photocatalysts with increased photocatalytic activity under light and antibacterial capabilities in the dark. [66]–[68]These catalysts may offer a less expensive option to noble metal-based bactericidal photocatalysts. [69] Researchers have recently shown the better visible-light-induced photocatalytic performance of copper, nickel, and iron-doped $TiO_2$ nanoparticles toward E. coli and S. aureus bacterium as a result of a study to evaluate the influence of metal ion doped in $TiO_2$ nanoparticles. [66], [70], [71]Nevertheless, the defect energy levels created in the $TiO_2$ band gap by the insertion of metal ions will potentially result in a reduction in the rate of recombination between photo-induced charge carriers. [69] Photocatalytic processes start when the electron transfer from the valance band to the conduction band of the photocatalyst and the hole will create as a result. Not all $TiO_2$ photocatalysts with metal doping will show promising results. The amount of dopant directly affects how quickly e/h+ recombination occurs[69].

### *2.6.2 Noble Metal Doping*

Another method for altering photocatalysts is the inclusion of noble metals. Silver, gold, and platinum were added to the $TiO_2$ photocatalyst to increase the noble metals' antibacterial action. [72] Since these noble metals' Fermi levels are lower than those of $TiO_2$, photogenerated holes in the valence band will leave $TiO_2$ while photoexcited electrons can be transported from the conduction band of $TiO_2$ to metal particles put on its surface. [72] As a

result, there is significantly less chance of electron-hole recombination, which leads to effective separation and increased photocatalytic properties[72].

Caballero et al. claimed that commercial $TiO_2$ powders doped with Pt have antibacterial action towards E. coli when exposed to fluorescent light. Platinum-doped $TiO_2$ photocatalyst demonstrated remarkable bactericidal activity because of the efficient distribution of $TiO_2$ nanoparticles and the improved charge separation in the loaded semiconductor photocatalyst[73].

Over the recent decades, a great deal of research has been done on silver modified $TiO_2$ photocatalyst materials. In the lack of light, silver is an established antimicrobial agent. [65] It has been suggested that the manner of bactericidal activity is related to the absorption of silver ions onto the negatively charged bacterial cell wall, which results in the inactivation of cellular enzymes, loss of permeability, and ultimately cell lysis and death. [65] The interfacial charge moves among noble metal and $TiO_2$ are highlighted as a photocatalysis-improving technique in the situation of noble metal composite $TiO_2$ photocatalysts. [65] This methodology may also help to cause photocatalytic inactivation besides the antibacterial and oligodynamic impacts of the embedded noble metals[65].

### *2.6.3 Non-metal Doping*

The partial replacement of oxygen with non-metals (N, C, and S) appears to be the most promising method now among the numerous chemical changes used to minimize the $TiO_2$ band gap. [65] There has been a lot of research on a non-metal doping approach to increase the bactericidal activity of $TiO_2$. [65] Many of the investigations have concentrated on non-metal doped $TiO_2$, which exhibits impressive photoactivity when illuminated with visible light. $TiO_2$ host lattice doping with non-metal ions (N, C, S, etc.) may cause a shift in the photocatalytic activity in the visible light region[65].

The band gap energy in the visible light spectrum is indeed shifted by carbon doping.

The visible light efficiency of carbon containing $TiO_2$ against several human pathogens, such as Staphylococcus aureus, Shigella Flexner, and Acinetobacter Baumann, was described by Cheng et al.[74] With the aid of confocal Raman spectroscopy and scanning electron microscopy, they additionally investigated how photocatalysts react with pathogens. Etacheri et al. investigated carbon-doped anatase brookite titania nano-heterojunction photocatalysts for S. aureus under visible light that were manufactured at low temperatures without the use of hydrothermal energy. They discovered that the band gap narrowing of the carbon-doped heterojunctions was caused by the interband C2p states[75].

# CHAPTER 3: A LITERATURE REVIEW OF MESOPOROUS SILICA NANOPARTICLES AND TOXICITY ASSESSMENT BY UTILIZING THE IN-VIVO MODEL (ZEBRAFISH EMBRYOS).

## 3.1 Introduction

Currently, a range wide of nanoparticle shapes have been created for biological applications, such as intracellular drug delivery and biomedical applications. [76]–[78] Mesoporous silica nanoparticles (MSNs) have become a potential and new drug delivery system for a variety of therapeutic compounds owing to their distinctive mesoporous structure, which maintains a level of chemical stability, surface functionality, and biocompatibility.[79] The Mobile Oil Corporation 1992 was produced for the first-time mesoporous silica materials and due to its unique textual characteristics, including its high surface area, huge pore volume, tunable pore diameter, and narrow pore size have drawn a lot of interest. [80] In addition, the mesoporous form of silica has interesting features for use in drug carriers, such as the ability to transfer bioactive molecules in high concentrations and transport the medication in a continuous and regulated manner, which results in a decreased overall in vivo cytotoxicity. [81]

## 3.2 Preparation of Mesoporous Silica Nanoparticles.

In an aim to create the structure of the structured mesophases that significantly rely on the interaction among the expanding anionic oligomers of orthosilicic acid and cationic surfactant, MSNs are synthesized at low surfactant concentrations. This reduces the size limits of the structure of mesophases.[24]

### *3.2.1 Manufacture of Mesoporous Silica Nanoparticles Using a Solution*

Mobile crystalline material (MCM-41) is the type of MSN that is utilized the most frequently; it is made up of cylindrical mesopores arranged in an ordered hexagonal pattern. Templating of cetyl trimethyl ammonium bromide, an alkyl ammonium salt is a necessary step in the synthesis of MCM-41 liquid crystal[82]. A spherical micelle made up of a high

concentration of amphiphilic surfactant forms in the presence of hydrophilic soluble precursors such as polyclinic acid or silica acid. The silica precursors are concentrated at the hydrophilic interface and form amorphous silica, which serves as a mold for the mesoporous product, through electrostatic and hydrogen bond interaction. The procedure of calcination and extraction can be used to remove any leftover surfactant[83].

### *3.2.2 Self-assembly Caused by Evaporation*

This process was introduced in 1997, starting with the formation of a homogenous solution of soluble silica and surfactant in ethanol and water, with a crucial micelle concentration of surfactant at first. To boost the concentration of the surfactant, the solvent evaporation process will begin during dip coating. [84] The subsequent production of liquid crystalline mesophases is driven by a silica/surfactant micelle mixture, as depicted in Figure 3a. Aerosol processing was used in the film-making process to control the creation of mesoporous nanoparticles. A non-volatile substance that can be added to an aerosol droplet integrated into the MSNs is evaporation-induced self-assembly[84].

### *3.2.3 Sol-gel Method*

Hydrolysis and condensation are two steps that must be considered in this process. Colloidal particles were created during hydrolysis and can be stimulated at both alkaline and acidic pH levels in an aqueous solution[85]. The condensation process occurs at neutral pH levels, and a gel-like 3D network structure is created by cross-linking with siloxane bonds. The various biomolecules became incorporated into a silica gel matrix after drying at room temperature, as depicted in Figure 3. Under the size range of 60-1000 nm, the (MCM-41) is formed during this process. The sol-gel technique has several benefits, including being a quick and affordable way to give MSNs tailored mesoporous structure and surface characteristics[86]. Since the sol-gel technique only requires one step, it saves time and uses fewer excipients (Figure 3b). [84]

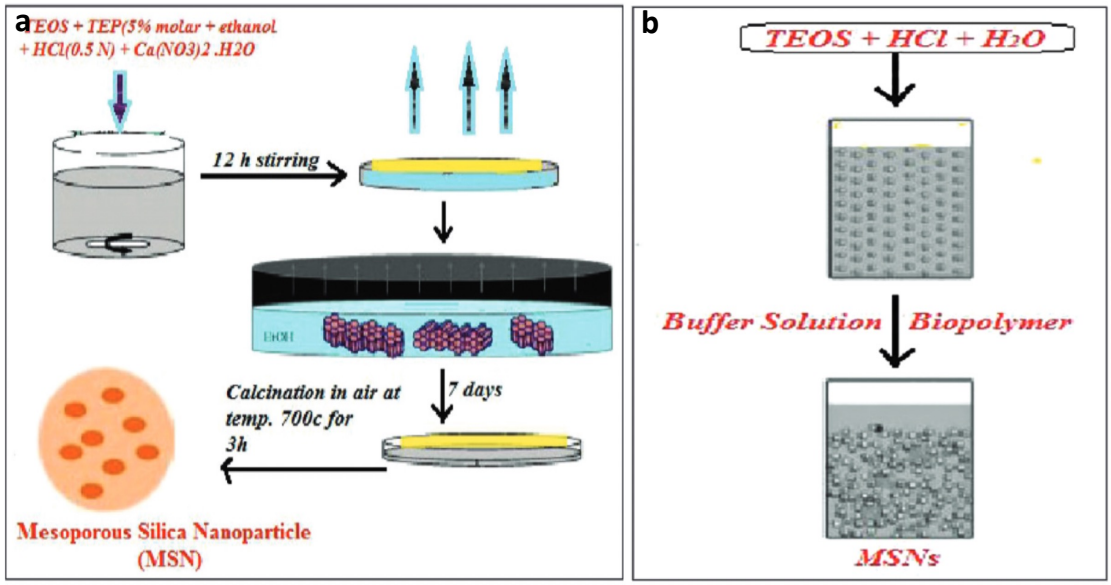


Figure 3. A synthesis method of mesoporous silica nanoparticles a) self-assembly caused by evaporation. b) sol-gel method.

## 3.3 Application of Mesoporous Silica Nanoparticles.

### *3.3.1 Drug Delivery*

In the late 1990s, discoveries of silica nanopore membranes led to the development of porous silica-based materials for drug carriers; one key benefit of the psi materials is that, according to the application. They may be designed for either continuous or triggered drug release. One of the earliest uses of this substance for drug administration was the paracellular distribution of insulin over a monolayer of intestinal Caco-2 cells. MSNs were widely utilized in drug delivery systems for the adsorption of harmful compounds due to their high surface area, selectivity of the adsorption component, and low toxicity. Activated carbon is typically used to eliminate harmful pollutants, although tests have shown that it is not very effective. [80]

Regular MSNs have a loading capacity of 200–300 mg (maximum 600 mg) drug/1 g silica per dose of therapeutic medication. For instance, the release of insulin is reduced over time in typical glucose-responsive insulin delivery systems. [80]

### *3.3.2 Mesoporous Silica Nanoparticles' Cellular Uptake*

Nanoparticles, made of mesoporous silica that are ingested by cells, have no discernible harmful consequences. [87] As the endocytosis of MSNs is blocked by lowering the temperature to 4°C and incubating the cells with metabolic inhibitors, the process of cellular uptake appears to be mediated by an active endocytosis route. The efficiency of the material's uptake by cells is noticeably improved by functionalizing MSNs' external surfaces with groups that cause cells to express particular receptor sites, such as folic acid, and by functionalizing the particles' zeta-potentials, which impacts both the efficiency of their internalization and the uptake pathway[88], [89].

### *3.3.3 Cell Tracking and Biosensing.*

Mesoporous silica nanoparticles are exploited as bio-sensing components because of their size and adaptable chemistry of structure. Thus, such nanoparticle-based sensor devices are employed for the in vivo and in vitro detecting of analysts throughout living cells. [90] Fluorescent, self-quenching, and other diffusion-related issues do not affect nanoparticles. As a result, a perfect agent for cell tracking can be created by functionalizing the surface of nanoparticles with significant amounts of cell recognition or other site-directing chemicals. [91]

### *3.3.4 Tumor-specific Targeting*

A novel and intriguing area of interdisciplinary research involving chemistry, medicine, material science, biology, and pharmacology is the use of porous silica materials for cancer therapy. To encourage the binding and internalization of nanocarriers, selective targeting technologies use ligands that specifically bind to receptors on the cell surface of interest. For this method to work, cancer cells must express receptors much more than healthy cells do. [92] Figure 7 illustrates how MSNs successfully cure malignant cells with drugs. The most interesting way to deliver medicine to a malignant cell is by surface

functionalization with targeted moieties, which is one of the great benefits of porous nanomaterials. [83]

Utilizing either direct interference with specific molecules associated with tumor growth and progression or indirect stimulation of the immune system to identify and eliminate cancerous cells, targeted MSNs therapies are employed to stop the growth and spread of cancer. [93] For instance, many harmful anticancer medications must first undergo "zero release" before they can reach the desired cells or tissues. Doxorubicin (DOX) can be efficiently delivered utilizing MSNs coated with a PEG copolymer, which can increase their size from 50 nm to 110 nm [94]. A KB-31 xenograft mouse received weekly injections of 120 mg/kg of nanoparticles for three weeks as part of the cancer treatment. 85% of tumors were inhibited by the DOX-loaded nanoparticles, relative to 70% by the free medication. [83]

### *3.4 Developing Virus-like Mesoporous Silica Nanoparticles.*

Since some viruses have a rough surface made up of spike proteins that may firmly adhere to cell membranes through the entrance process, it has been shown that some viruses have good cellular invasion capabilities. A few recent studies have been conducted to create nanomaterials with the topological structures of viruses, which were inspired by the distinctive surface morphology of viruses.[24], [95]–[97] It is crucial to enhance the cellular uptake of mesoporous silica nanoparticles, therefore fabricating virus-like-structured porous particles with perpendicular spiky nanotubes to satisfy the demands of effective cellular reception in different biological applications. Recently, uniform virus-like mesoporous silica nanoparticles with inner mesoporous nanospheres encircled by epitaxial perpendicular mesopore nanotubes have been successfully created in an oil/water biphase reaction system with low surfactant concentrations by using hexadecyltrimethylammonium bromide (CTAB) as a structural template and tetraethyl orthosilicate (TEOS) as a precursor. [24] These distinct nanotubes generate a rough surface structure resembling the spike proteins of viruses as they

develop radially from the interior mesoporous silica nanospheres. However, the discovered mesoporous silica nanoparticles have the highest of cellular absorption rate, which can be attributed to the rough surface that resembles a virus and allows them to infiltrate living cells in vast numbers within 5 minutes. [24] The virus-like mesoporous silica nanoparticles exhibit distinct internalization pathways and have blood circulation (t1/2 = 2.16 h) that lasts substantially longer than conventional mesoporous silica nanoparticles (0.45 h). The doxorubicin (DOX)-loaded virus-like nanoparticles exhibit significantly increased tumor cell cytotoxicity, indicating significant promise for biomedical application[24].

### 3.5 Cytotoxicity Evaluation by Utilizing Zebrafish Embryos.

High-throughput and inexpensive animal models are receiving more attention in biomedical fields including toxicity assessment and drug screening. The zebrafish embryo is a common illustration of these models [98]. The embryo of the zebrafish (Danio rerio) merges biological research in animals including rats and easy tests involving cell culture. In other words, the zebrafish embryo model has essential features including tiny size, visibility, rapid organ growth, short, tested period, easy manipulation, direct substance distribution, and little amount of the tested samples needed. Furthermore, genomic sequencing has shown the extensive similarity between zebrafish and other vertebrate species, including humans, and has also shown that characteristics of brain anatomy and patterning with function are preserved. [99] Zebrafish and their embryos have been used successfully in publications to forecast human toxicity and cytotoxicity consequences. The US Food and Drug Administration (FDA) and the European Medicines Evaluation Agency (EMEA) have both approved the use of zebrafish in safety and toxicity assessments for the assessment of novel drug authorization. Previous research claimed that the survival percentage of zebrafish treated with mesoporous silica nanoparticles was reported to be above 85%. Other investigators found that the highest NOEC evaluated by the acute toxicity assay for the core-shell magnetic

mesoporous silica microspheres was 1.6 mg/mL. [100]

# CHAPTER 4: MATERIAL AND EXPERIMENTAL METHOD

## 4.1 List of Material

The chemicals used in all experiments are listed in Table 1 below:

Table 1. List of chemicals and reagents used in the experiments.

| Material | Manufacturer |
|---|---|
| Titania rutile, $TiO_2$ | AEROXIDE |
| Silver nitrate, $AgNO_3$ | HIMEDIA |
| Nickel II nitrate 6-water, $Ni(NO_3)_2 . 6H_2O$ | Breckland Scientific |
| Sodium borohydride, $NaBH_4$ | Fisher Scientific |
| Ethanol, EtOH | Fisher Chemicals |
| Ultra-pure water, UPW; 18.1 MΩ-cm | Thermo Scientific |
| Hexadecyltrimethylammonium bromide, CTAB | Sigma-Aldrich |
| Sodium hydroxide, NaOH | VWR chemicals |
| Cyclohexane, $CH_6$ | Shanghai Chemical Co., Ltd |
| Tetraethyl orthosilicate, TEOS | Aladdin Industrial Inc |
| Luria-Bertani broth, LB broth | Sigma-Aldrich |
| N-Phenylthiourea, PTU | Sigma-Aldrich |
| Zinc oxide, ZnO, suspension nanparticles | Sigma-Aldrich |
| Pronase | Sigma-Aldrich |

All purchased chemicals were used as manufactured without further purification.

## 4.2 Experimental Procedures

### *4.2.1 Synthesis of NiO/Ag/$TiO_2$ Catalyst*

For the first time, the co-precipitation method was used to create the ternary nanocomposite 1% NiO/Ag/$TiO_2$ . Basically, A 250 ml beaker containing 4 g of $TiO_2$ (rutile) nanopowder was combined with 150 ml of ultrapure (UP) water and absolute ethanol at a volume ratio of 1:1. The mixture was then dispersed for 15 minutes with an ultrasonic probe. Ag and Ni content were mixed at a ratio of 0.6:0.4. Thus, 0.0377 g of Ag ($NO_3$) and 0.0793 g of Ni ($NO_3$) were individually mixed in 20 ml of the combined solution of ultrapure (UP) water and absolute ethanol at a volume ratio of 1:1 for 15 minutes. The solutions were added to the $TiO_2$ solution later, and it was stirred for 15 minutes. Then, using the titration method, 0.1 M $NaBH_4$ was added to the solution drop by drop until the white solution turned to light brown color. The amount of $NABH_4$ was around 8ml, acting as a strong reducing agent. However, to avoid the high reactivity of $NABH_4$ before adding it to the solution was kept in an ice bath. The solution was then agitated for an hour. The nanopowder was then separated by centrifuging. The sample was then dried in an oven at 60 $^oC$ for 24 hours after being cleaned three times by ultrapure (UP) water and 100% of ethanol. Furthermore, the other monometallic/$TiO_2$ (1% Ag/$TiO_2$ and 1% Ni/$TiO_2$) were produced using the same guidelines and methods of the above procedures.

### *4.2.2 Methylene Blue Photocatalytic Activity*

To assess the catalyst's functionality, an aqueous solution of the Methylene blue (MB) dye was utilized. A 400W ( $\lambda \geq 400$) halogen lamp is permanently used to emit visible light, with an average intensity of 1413.4W/m2 in all photocatalytic experiments. The lamp's distance from the beaker was 15 cm. A solution of 80ml MB (5.0 mg/L) was mixed with several quantities of photocatalyst (0.02, 0.04, and 0.08g) in a 150ml beaker. To achieve equilibrium in the absorption and desorption processes involving the produced photocatalyst and the MB, the solution was agitated in the dark for 30 minutes. The MB’s maximum

wavelength absorption was obtained at 664 nm by using the UV-visible spectrometer. To assess MB dye breakdown, the absorbance was monitored for 60 minutes at 10-minute intervals. Moreover, the aqueous solution was subjected to radiation in the control experiment without the use of a photocatalyst. The blank in each experiment consisted primarily of UP water. After separating the photocatalyst from the MB solution via a 0.45 m PTFE syringe filter throughout the experiment, the MB was examined utilizing a UV-visible spectrometer. The following equations were employed to calculate the efficiency of the degradation as well as the kinetic model of the MB dye degradation reaction:

$$\ln(C/C_0) = Kt \quad (1)$$

The pseudo-first-order kinetics states that K is the reaction rate constant, C is the concentration of MB at time t, and C0 is the initial concentration of MB.

$$R = \left(1 - \frac{C}{C_0}\right) \times 100\% \quad (2)$$

R is the photocatalytic efficiency, Co is the beginning reactant concentration of the aqueous MB solution, and C (g/L) is the final reactant concentration of the aqueous MB solution.[101].

### *4.2.4 Pharmacratic Degradation (Aspirin and Paracetamol)*

The exact experimental setup and circumstances utilized for MB dye degradation were applied to the photocatalytic degradation of medicinal substances. Aspirin (ASP) and paracetamol (PCL) were utilized as the pharmaceutical waste to assess the nano catalyst's effectiveness at degrading medicinal waste. Each of the pharmaceutical substances was treated at a concentration of 2 ppm, while the catalyst was utilized at a concentration of 1 g/L. The UV-visible spectra at 197 nm was used to calculate the absorbance maximum wavelength. A 0.45-m Millipore filter was used to filtrate the solution to remove the photocatalytic particles.

### *4.2.5 Anti-bacterial Assay*

First, the solutions were prepared with the nanomaterial ($NiO/Ag/TiO_2$) with

different concentrations of 1, 0.5,0.2 g/L and sonicated with LB Broth media for 10-15 min. Second, for the bacteria, two different types have been used (E-coli & Staph aureus). For the two types: one well-isolated colony has been chosen then, diluted with the LB Broth in tubes by using a vortex, and put in an incubator with shaking for 18 hours at 37 C to grow the bacteria. After that, 50 uL from the Ecoli and S.aureus were added to each tube and kept in the incubator with shaking. The tubes that are in dark condition were covered with tinfoil. The absorbance reading will take each hour for 5-6 hours until the bacteria reach the stationary phase. For each dosage, the absorbance was taken in three replications with an optical density (OD) of 600 nm. The average of three measurements versus time (hr) for each concentration was used to graph the OD values. This investigation was repeated three times. All experiment calculations were done by using Origin software (2018 version).

### *4.2.6 Synthesis of Mesoporous Silica Nanoparticles*

A previously identified technique was used to synthesize silica nanoparticles with mesopores that resemble viruses[24]. In most cases, TOES was used as a source of silica, NaOH served as the catalyst, and cyclohexane served as the immiscible phase. First, 50 mL of water, 1 g of CTAB, and 0.8 mL of NaOH (0.1 M) were combined in a flask with a round bottom. The solution was kept string for two hours. After that, 20 mL of mixed TEOS in cyclohexane (4 mL of TEOS in 16 mL of cyclohexane) was added to the mixture and held at 60 °C with agitation for 48 hours. The layers are centrifuged apart and washed three times with ethanol and water. Next, the powder was immediately added to 50 mL of acetone and refluxed for 12 hours at 50 °C to remove CTAB templates. After washing with ethanol, the specimens were dried in a furnace for 8 hours at 45 °C.

### *4.2.7 Zebrafish Toxicity Assay*

Acute toxicity tests were conducted using the wild-type zebrafish AB strain. The

Institutional Animal Care and Use Committee (IACUC) of Qatar University approved the rules and procedures for all zebrafish investigations. Healthy, deformity-free embryos were chosen at 24-hour postfertilization (hpf). Zebrafish embryos (20 embryos/concentration) were incubated in PTU prepared by adding 0.5 mg/mL pronase enzyme for 10 minutes to dechorionated the embryos. After that, three PTU solution washes were performed on the embryos. The embryos are now ready to be tested by directing the substances that want to be studied. The 20 embryos per well were transferred to two of a 6-well plate. Distinct concentrations of V-MSN (200, 400, 600, 800, 1000, 1200, 1400, and 1600 mg/L), 40 mg/L of ZnO nanoparticles (negative control) that dissolved in PTU and PTU only as a positive control. The 6-well plates were kept at 28 $^{o}$C for incubation till 96 hpf. Using a ZiessStemi2000-C stereomicroscope, the survival rate and morphological abnormalities (teratogenic effect) were detected and documented at 96 hpf. 6 embryos were selected randomly from each concentration to measure the teratogenic effects (body length, yolk, heart, and eye sizes). The images were taken by utilizing a high-speed camera called the Hamamatsu Orca Flash that was connected to a Zeiss SteREO Discovery V8 microscope which is already linked to the screen by HCImage software, version 4.4.1.0. (Hamamatsu Photonics, Tsukuba, Japan). The median lethal dose (LC50) was found by drawing a sigmoidal curve to mortality data utilizing GraphPad Prism 7 software. All the graphs for the zebrafish experiment were obtained by GraphPad Prism 7 software.

### 4.3 Characterization

The $N_2$-sorption assessment utilizing Micromeritics' ASAP2020 Accelerated Surface Area and Porosimetry System (Micrometrics, Norcross, GA, USA) and the Brunauer-Emmett-Teller (BET) and Barrett-Joyner-Halenda (BJH) techniques were used to calculate specific surface area and the pore size distribution, respectively at 77K. X-ray diffraction (XRD) (PAN Analytical Empyrean) was used to analyze the structure, crystallography, and

phase of the produced catalyst for the photocatalyst throughout a temperature range of 10° to 99.9°. The transmission Electron Microscope (TEM) and scanning electron microscopy (SEM) were made by (FEI) (TECNAI G2 TEM, TF 20). To study the morphology and elemental composition of the catalysts that were created, high-resolution transmission electron microscopy (HRTEM) was carried out manufactured by (FEI Talos 200X) operated at 200 kV and energy-dispersive (EDS) (Thermofisher Scientific, USA). The concentration and surface state of the elements of the composite's nanoparticles were determined using X-ray photoelectron spectroscopy (XPS; Omicron Nanotechnology, Germany), and Casa XPS software was used for data processing and peak fitting. The XPS spectra, that were obtained, were calibrated to the 284.6 eV C1s feature. A split-beam UV-visible spectrophotometer (YK Scientific, UV1810/UV1810S, China) was used to measure the UV-visible absorption spectra of the manufactured samples. Total organic carbon (TOC) was used by Formacs analyzer (Breda, The Netherlands) instrument to find the reduction of the carbon compound of MB before and after adding the catalyst.

# CHAPTER 5: SYNTHESIS AND CHARACTERIZATION OF NiO/Ag/$TiO_2$ TERNARY NANOCOMPOSITE AND PHOTOCATALYTIC ACTIVITY ON MB DYE AND PHARMACEUTICAL WASTES AND BACTERICIDAL UNDER VISIBLE LIGHT IRRADIATION.

## 5.1 Catalyst Characterization

The 1% NiO/Ag/$TiO_2$ nanocomposite's XRD pattern was shown in Figure 4. Tetragonal rutile $TiO_2$16-like diffraction peaks can be seen in the XRD pattern. As seen in Figure 4, the rutile $TiO_2$ reflection of (110), (101), (111), (210), (211), (220), (002), (310), (301), and (112) are matched to the diffraction peaks at 2θ = 27.74°, 36.42°, 41.58°, 44.40°, 54.64°, 56.56°, 63.09°, 64.20°, and 69.83°, respectively. Due to the small amount of Ag and Ni dopants and their uneven distribution on the $TiO_2$ surface, there are few signals for Ag0 and NiO. In general, the reflection peaks were accurately attributed to tetragonal rutile $TiO_2$ with no evidence of any other $TiO_2$ phase, as well as to Ag and NiO without any indication of Ni metal signals.

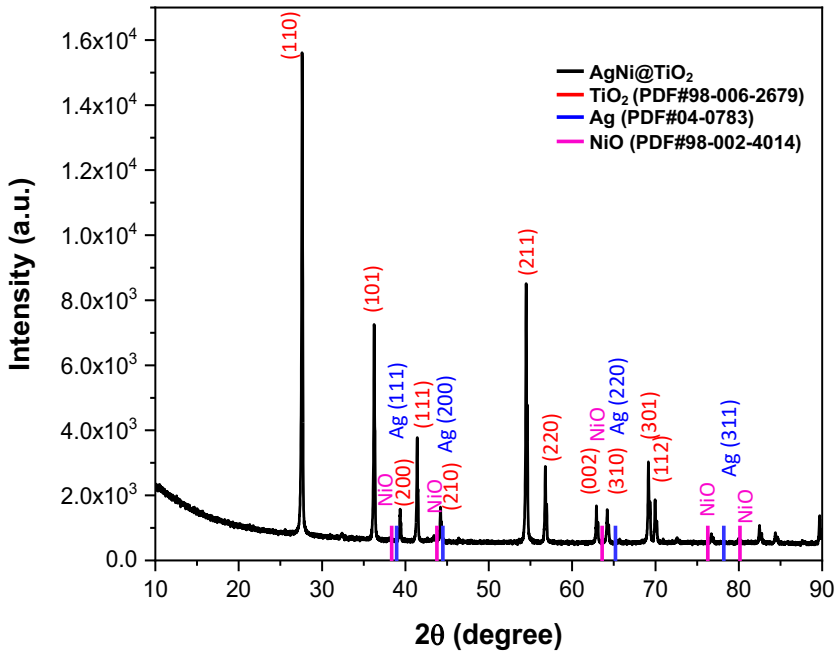


Figure 4. XRD patterns of NiO/Ag/$TiO_2$ nanoparticles.

The 1% NiO/Ag/$TiO_2$ nanocomposite was investigated by utilizing XPS as shown in Figure 5. Figure 5 (a) shows the survey spectrum of the analysis of the material's chemical components. XPS peaks demonstrate that the material has minimal contamination and contain Ni 2p, Ti 2p, Ag 3d, O 1s, and C 1s from the XPS instrument. The Ti(2p) binding energy region had two peaks, as shown by Figure 5 (b)–(e). While the Ti(2p3/2) is assigned to the peak at 459.1 eV, the Ti(2p1/2) is credited to the peak at 464.7 eV. Ti4+ is in a normal state, as evidenced by the 5.6 eV split between the Ti(2p1/ 2) and Ti(2p3/2) core levels. Furthermore, the Ni 2p scan peaks at 873.2 eV and 855.6 eV, which are attributed to the Ni 2p1/2 and Ni 2p3/2 signals, respectively, show the formation of the Ni-O bond. There is no peak appearance to prove the presence of metallic Ni (852.7eV), which confirmed that there is a layer of completely Ni oxidative on the top. Deconvolution of the Ag 3d5/2 and Ag 3d3/2 spectra at binding energies of 368.3 eV and 374.3 eV are visible in the Ag 3D scan and slicing of the Ag 3d doublet at 6.0 eV reveals the occurrence of Ag0 (metallic Ag).

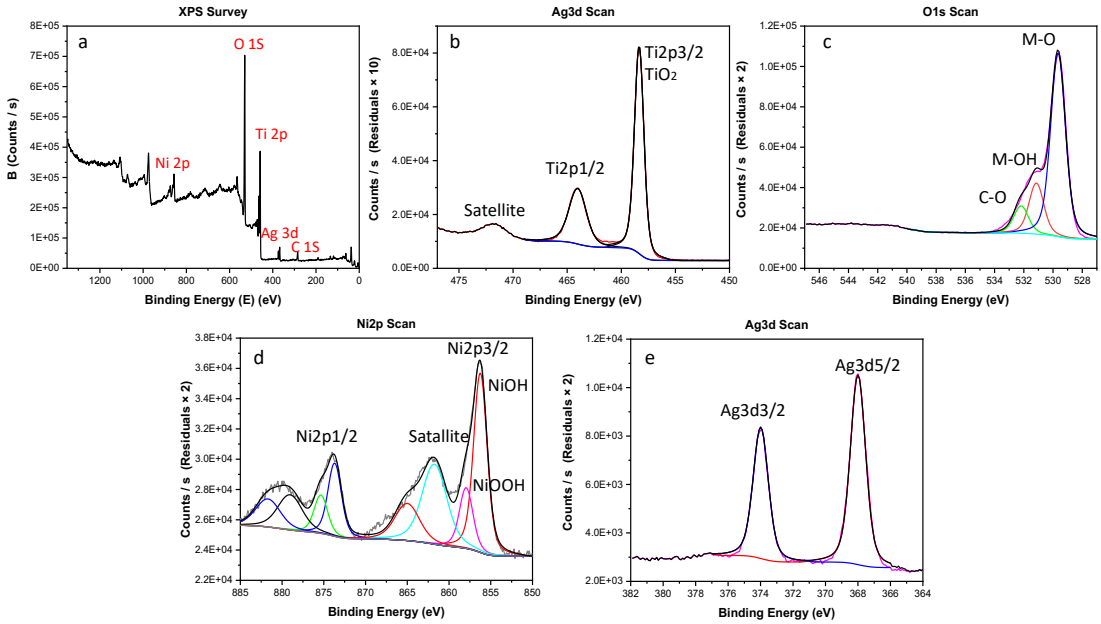


Figure 5. XPS analysis of 1% NiO/Ag/$TiO_2$ : (a) survey spectrum and high-resolution spectra (b) Ag 3d, (c) O 1s, (d) Ni 2p and (e) Ti 3d.

Figure 6 shows images at a high-resolution Transmission Electron Microscope (HRTEM) of an AgNi@$TiO_2$ nanocatalyst. Figures 6(a-c) illustrate the typical spherical form and size of $TiO_2$, which range in size from 150 to 200 nm. According to HRTEM, the majority of the Ag nanoparticles are small, evenly dispersed (3 nm) and some larger Ag nanoparticles (3-10 nm) are adhered to and growing on the $TiO_2$ surface. The oxidation of Ni cannot identify regarding the HRTEM.

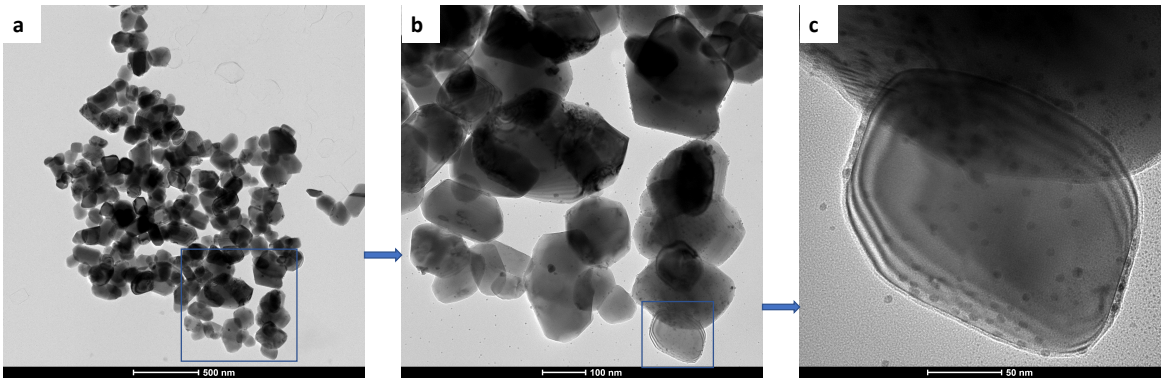


Figure 6. High-resolution Transmission Electron Microscope (HRTEM) of NiO/Ag/$TiO_2$ (a-c).

Ascribed to Figure 7, the TEM-EDS mapping used to study the morphology, shape, size, and distribution of the Ag and Ni particles on $TiO_2$ nanoparticles. Quantitative EDS mapping used to show the distribution of the silver and Nickel on $TiO_2$ in Figure 7(a). Figure 7(b-f) demonstrates the elemental mapping of Ag, Ni, Ti, and O by using scanning TEM (STEM)–high-angle annular dark field (HAADF). These findings show the good distribution of Ag and Ni oxide on the surface of $TiO_2$.

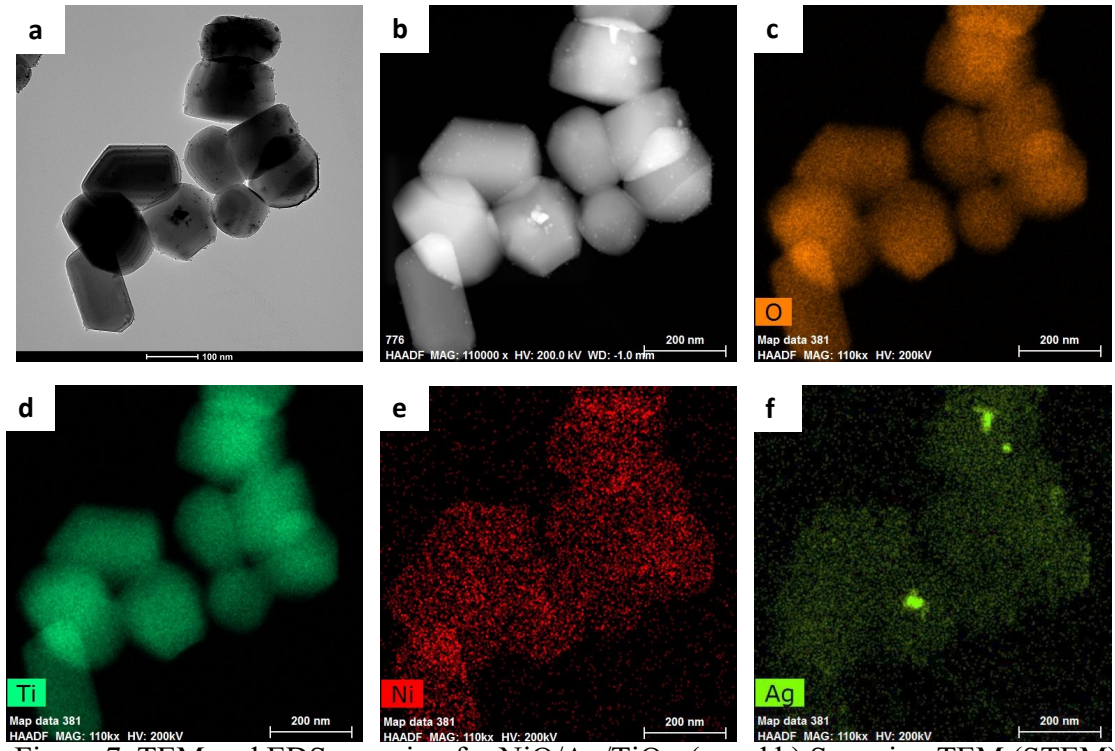


Figure 7. TEM and EDS mapping for NiO/Ag/$TiO_2$. (a and b) Scanning TEM (STEM)–high-angle annular dark-field (HAADF) and light-field(HAALF); (c-f) Elemental distribution mapping of NiO/Ag/$TiO_2$.

## 5.2 Study of the UV-visible Spectra

The comparison of the findings of the group of synthesized nanoparticles of (bare $TiO_2$ (rutile), 1% NiO/Ag/$TiO_2$, 1%Ag/$TiO_2$, and 1%Ni/$TiO_2$) was examined by UV-visible spectroscopy as illustrated in Figure 8. The optical characteristics and the energy gap of the 1% NiO/Ag/$TiO_2$ photocatalyst were analyzed, which was determined in the (300-900 nm) wavelength range Figure 8(a). When compared to TiO2 and other composites like Ag/TiO2 and Ni/TiO2, the NiO/Ag/$TiO_2$ nanoparticles exhibited the largest shift to the right (redshift), as shown by the results in Figure 8(a). The redshift results in a higher wavelength and lesser energy. Thus, the insertion of Ni and Ag nanoparticles in TiO2 has improved the composite in general. Moreover, the energy bands were calculated for NiO/Ag/$TiO_2$, $TiO_2$, Ag/$TiO_2$, and Ni/$TiO_2$ which are 1.9, 2.6, 2.1, 2.3 eV respectively by utilizing the Tauc's plot method as

shown in (Figure 8(b)). The composite of heterogeneous NiO/Ag/$TiO_2$ nanoparticles has an energy gap of 1.88 eV, which is close to our findings according to prior research. As well as NiO/Ag/$TiO_2$ nanoparticle has the lowest energy band, therefore the energy that needs to transfer the electrons from the valence band to the conduction band is lower than the energy that needs for Ag/$TiO_2$, Ni/$TiO_2$, and $TiO_2$ nanoparticles. As a result, adding Ni and Ag nanoparticles to $TiO_2$ improves the composite as a whole. Additionally, using the Tauc's plot approach, it was determined that the energy bands for NiO/Ag/$TiO_2$ , $TiO_2$, Ag/$TiO_2$, and Ni/$TiO_2$ are 1.95, 2.5, 2.22, and 2.15 eV, respectively (Figure 8(b)). Additionally, the NiO/Ag/$TiO_2$ nanoparticle has the lowest energy gap; therefore, it requires less energy than Ag/$TiO_2$, Ni/$TiO_2$, and $TiO_2$ nanoparticles to excite electrons to move from the valence band to the conduction band.

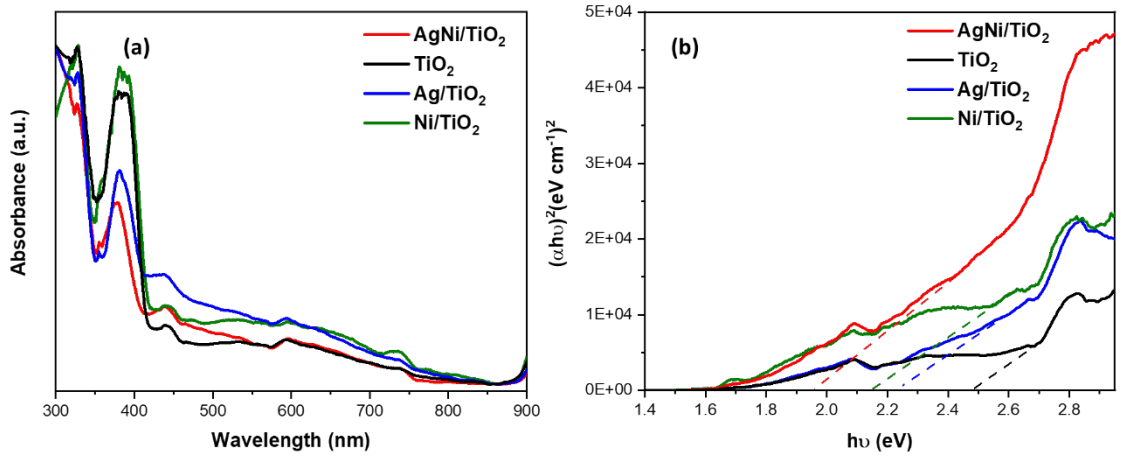


Figure 8. (a) A comparison of Ag/$TiO_2$, Ni/$TiO_2$, NiO/Ag/$TiO_2$, and $TiO_2$ UV-visible spectra. (b) The band gaps of the composites by using the Tauc plot are related to the UV-vis spectra.

## 5.3 Analysis of the MB Dye Solution Photodegradation

### *5.3.1 Comparison of the Photodegradation of 1% NiO/Ag/$TiO_2$ and Other Nanocomposites*

Underneath the influence of visible light, NiO/Ag/$TiO_2$ nanocomposite and other materials' photocatalytic degradation of methylene blue dye solution were investigated. In

aqueous methylene blue dye (1 g/L), 1% NiO/Ag/TiO2 , 1% Ni/TiO2, 1%Ag/TiO2, and bare TiO2 were investigated as photocatalysts for 60 minutes. As depicted in Figure 9a, the absorbance was calculated as a function of time using (Ct/C0) versus time (minutes). According to the results, 1% $Ag/TiO_2$ had the highest photocatalytic reactivity of all the compounds examined, with a (Ct/C0) value of (0.068) at 60 minutes, which is near zero. According to Figure 9b, the ln Ct/C0 was plotted against the reaction time for all the investigated nanocomposites and MB without a catalyst. By using a fit linear equation in accordance with the pseudo-first-order kinetics law, the slopes for the compounds were determined as the reaction rate (k). The degradation efficiency and reaction rate constant for each nanocatalyst are summarized in Table 2. 1% $NiO/Ag/TiO_2$ had the highest degrading efficiency (93.15%) and the fastest reaction rate (0.03121 $min^{-1}$) of all the investigated compounds (1%$Ni/TiO_2$, 1%$Ag/TiO_2$, and bare $TiO_2$). In contrast to existing composites on $TiO_2$ and bare $TiO_2$, the unique nanocomposite catalyst (1% $NiO/Ag/TiO_2$) has the best photodegradation rate for MB aqueous solution. In addition, according to earlier investigations, G-P25, $GTiO_2$, G-ZnO, and G-ZnO-CTAB reached 100% photodegradation of MB aqueous solution in 80, 110, 90, and 150 minutes, respectively, in the same conditions[102]. However, 1% $NiO/Ag/TiO_2$ degraded 100% of MB solution at around 63 minutes, according to the fitted linear equation. Furthermore, recent research has shown that 1% $Ag/WO_3$ photocatalyst deteriorated the MB aqueous solution by roughly 76.6% in 60 minutes under the same conditions[103]. In comparison to the previous catalysts, 1% $NiO/Ag/TiO_2$ demonstrated the best degrading efficiency of MB aqueous solution and is expected to garner considerable interest in the catalysis community.

Table 2. The rate constants of the decomposition of MB reaction and the efficiencies for bare $TiO_2$, $NiO/Ag/TiO_2$ , $Ni/TiO_2$, $Ag/TiO_2$ photocatalysts, and MB without catalyst.

| Material | The reaction rate constant ($min^{-1}$) | Degradation efficiency (%) |
|---|---|---|
| 1% $NiO/Ag/TiO_2$ | 0.03121 | 93.15 |
| 1%$Ni/TiO_2$ | 0.00542 | 39.4 |
| 1%$Ag/TiO_2$ | 0.01733 | 76.73 |
| Bare $TiO_2$ | 0.01112 | 60.7 |
| No-catalyst | 0.00269 | 19.3 |

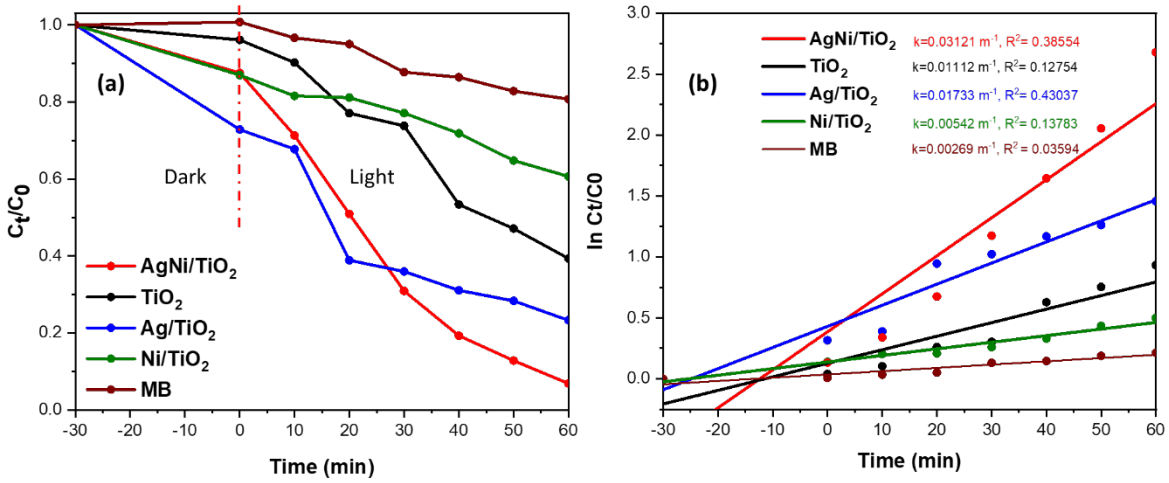


Figure 9. Photocatalytic degradation of MB solution. (a) A comparison of $NiO/Ag/TiO_2$ , $TiO_2$, and other monometallic/$TiO_2$ composites under visible light irradiation for 60 minutes (b) Pseudo-first order kinetics of the decomposition of MB aqueous solution.

### *5.3.2 Kinetics Analysis of the Relationship Between Photocatalyst Dose and Photocatalytic Performance.*

The amount of catalyst utilized has a great effect on how well a pollutant is photodegraded. Less catalyst-intensive degradation methods are preferred. In this study, the efficiency of the photodegradation of MB aqueous solution was tested using 0, 0.2, 0.5, and 1 g/L dosages of $NiO/Ag/TiO_2$ nanocomposite catalyst with the presence of visible light

within 60 minutes. For 1 g/L of NiO/Ag/$TiO_2$ photocatalyst, the absorbance reading vs wavelength was plotted, as seen in Figure 10a. This was accomplished dynamically by monitoring the catalyst accelerating MB's breakdown for 60 minutes for the whole doses of 1% NiO/Ag/$TiO_2$. It displays the highest absorption at 664 nm wavelength. Figure 10b depicts the achievement of the (0–1 g/L) dosages of the NiO/Ag/$TiO_2$ nanocomposite catalyst as a function of concentration (Ct/C0) and time (min). It demonstrates that the photodegradation activity of the MB solution increases in the following sequence as the doses of the catalyst increment: 0, 0.2, 0.5, and 1 g/L of the catalyst. Through employing the pseudo-first-order kinetic equation of ln Ct/C0 versus time (min), the corresponding kinetic data of MB dye solution photocatalytic degradation by the different doses of NiO/Ag/$TiO_2$ nanoparticles were obtained in Figure 10c. Table 3 lists the degradation efficiencies and reaction rate constants for 1% NiO/Ag/$TiO_2$ photocatalysts at various dosages (0, 0.2, 0.5, and 1 g/L) in MB aqueous solution for 60 minutes of visible light. Obviously, the 1 g/L dose of the catalyst had the greatest impact on the photodegradation of the MB solution with a reaction rate constant of 0.0319 $min^{-1}$, which is 1.7 times quicker than the 0.2 g/L doses of the catalyst and 11.8 times faster than the MB solution without the catalyst. Additionally, for the catalyst doses of 0, 0.2, 0.5, and 1 g/L, the respective degradation efficiencies are 93.19, 79.71, 56.85, and 19.3%. Hence, the 1% NiO/Ag/$TiO_2$ photocatalyst is considered dose-dependent, and even when using a little amount of it (0.2 g/L) it exhibited a well-increasing in the velocity of the degradation. Additionally, Figure 10(d) illustrates the relationship between the rate constant of MB solution photodegradation and the concentration of 0-1 g/L of 1%AgNi@$TiO_2$. According to the data, the rate constant for the photodegradation reaction was 0.0281 $min^{-1}$ for 1% NiO/Ag/$TiO_2$ and 0.0111 $min^{-1}$ for $TiO_2$ photocatalyst, which is 2.6 times faster in the same circumstances.

Total organic carbon (TOC) was measured for additional characterization of MB aqueous solution to determine the quantity of carbon present both before and after 60 minutes of visible light irradiation with a catalyst with a concentration of 1 g/L of 1% NiO/Ag/$TiO_2$ nanoparticles. Before the catalyst was added, the solution's total carbon concentration was 85.63 mg/L and it was 6.07 mg/L after apparent the catalyst was in the solution within 60 minutes. To remove the excess catalyst, the solution was centrifuged before testing. Therefore, after 60 min of visible light irradiation, the elimination of TOC is 92.91% when employing 1% NiO/Ag/$TiO_2$ nanoparticles as a photocatalyst. In conclusion, the material's ability to degrade the MB solution validates its remarkable photocatalytic activity.

Table 3. The rate constants of the decomposition of MB reaction and the efficiencies of 1% NiO/Ag/$TiO_2$ photocatalysts using different doses (0, 0.2, 0.5 and 1 g/L)in MB aqueous solution within visible light for 60 minutes.

| Dosage (g/L) | The reaction rate constant ($min^{-1}$) | Degradation efficiency (%) |
|---|---|---|
| 0 | 0.0027 | 19.3 |
| 0.2 | 0.0188 | 56.85 |
| 0.5 | 0.0244 | 79.71 |
| 1 | 0.0319 | 93.19 |

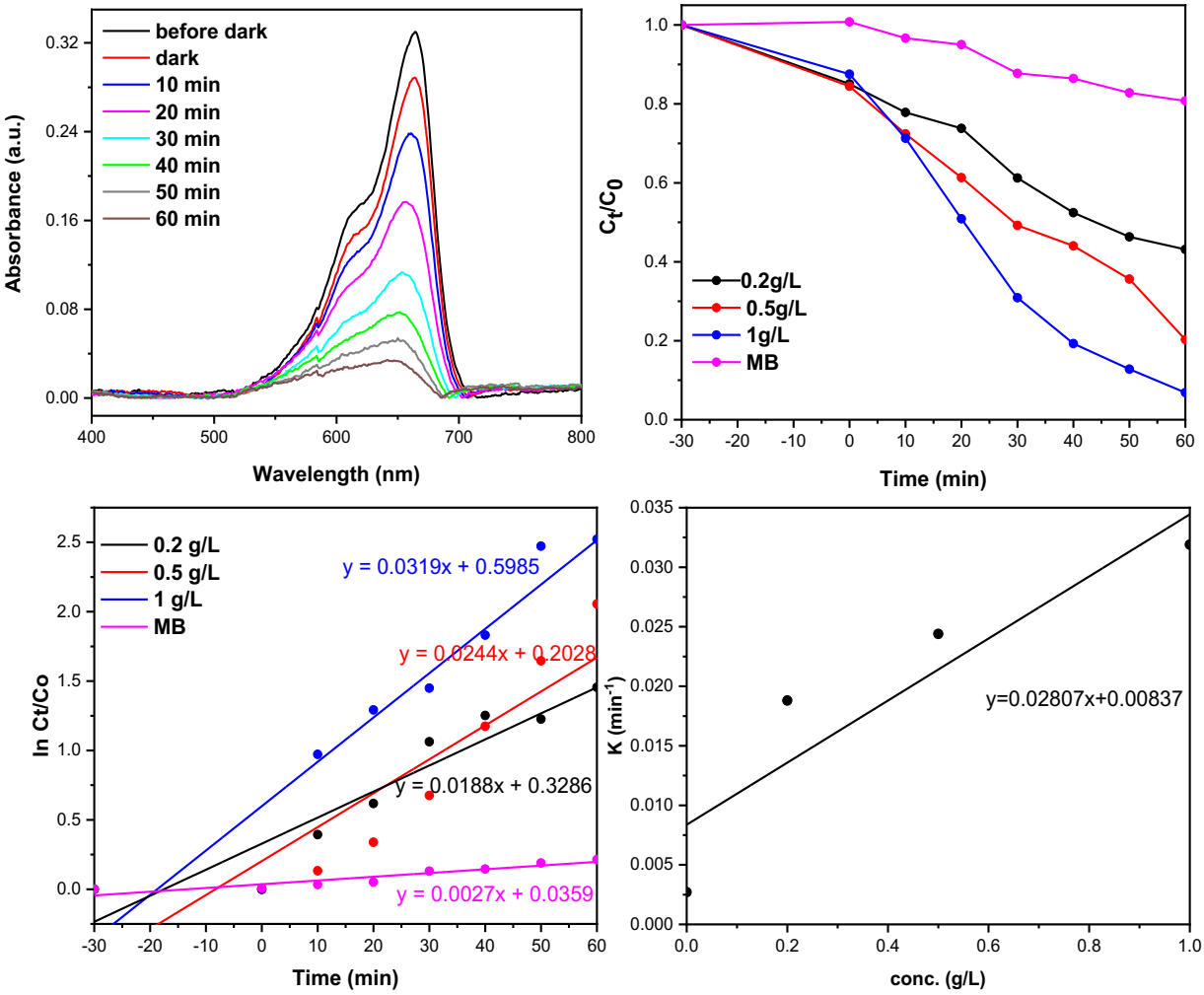


Figure 10. (a) UV-vis absorption spectra of MB solution with time-dependent deterioration in 1% NiO/Ag/$TiO_2$ presence under visible light illumination. (b) Varied concentrations of 1% NiO/Ag/$TiO_2$ (0-1 g/L) photodegraded MB solution within 60 minutes within visible light irradiation. (c) Pseudo-first order kinetics for the decomposition of MB solution via 1% NiO/Ag/$TiO_2$ (0-1 g/L). (d)The constant rate of the deterioration of MB solution versus the concentration of 1% NiO/Ag/$TiO_2$ (0-1 g/L).

## 5.4 Impact of Annealing Treatment

The nanostructure material's thermal treatment can improve its structural, morphological, electrical, and optical properties [104]. According to Sugapriya et al., bare $TiO_2$ and Ag/$TiO_2$ had enhanced crystalline structure and phase change after annealing treatment [105], [106]. Figure 11 (a and b) showed the MB dye solution's photocatalytic

degradation by NiO/Ag/$TiO_2$ before and after annealing, both at 600 °C for two hours. The identical set of circumstances used in all the tests in this work was used to test the photocatalytic performance. Figure 11(a) shows the ratio of (Ct/C0) vs reaction time (min) for the MB photocatalytic degradation with 1 g/L for each 1% NiO/Ag/$TiO_2$ with annealing, 1% NiO/Ag/$TiO_2$ without annealing, and MB with no catalyst. In accordance with Figure 11(a), 1% NiO/Ag/$TiO_2$ with an annealing curve demonstrated a better photodegradation of MB (Ct/C0) decline than 1% NiO/Ag/$TiO_2$ without an annealing curve. The pseudo-first-order kinetics that was fitted to the MB solution degradation data are shown in Figure 11(b). It demonstrates the reaction rate constant of the 1% NiO/Ag/$TiO_2$ with an annealing curve was faster (0.03635 min-1) than that of the 1% NiO/Ag/$TiO_2$ without annealing (0.03121$min^{-1}$). Table 4 lists the reaction rates and the degradation efficiency, revealing that the annealed nanocomposite catalyst performed better in the photodegradation activity, obtaining a degradation efficiency of 95.92% as opposed to 93.15% for the non-annealed nanocomposite catalyst. To improve the characteristics of the nanocomposite catalyst, heat treatment was applied. This leads to increased surface roughness, crystallinity, and reduced band gap of the nanocomposite, which indeed increases the photocatalytic activity of the MB dye solution [107]. Additionally, heating causes stress to decrease because of the larger Ag atoms and the segregation of Ag atoms to the catalyst's surface owing to Ag's reduced surface energy. The significant cohesive energy of silver nanoparticles and the low interaction energy of silver with NiO and $TiO_2$ enhance the motion of silver atoms on the nanocomposite surface and cause Ag nanoparticles to aggregate. This phenomenon was shown in Ag/$TiO_2$ nanocomposite[108].

Table 4. The rate constants of the decomposition of MB reaction and the efficiencies via 1% $NiO/Ag/TiO_2$ without annealing treatment and 1% $NiO/Ag/TiO_2$ with annealing treatment catalyst, and MB without catalyst with the presence of visible light for 60 minutes.

| Material | The reaction rate constant ($min^{-1}$) | Degradation efficiency (%) |
|---|---|---|
| No-catalyst | 0.00269 | 19.3 |
| No annealing | 0.03121 | 93.15 |
| With annealing | 0.03635 | 95.92 |

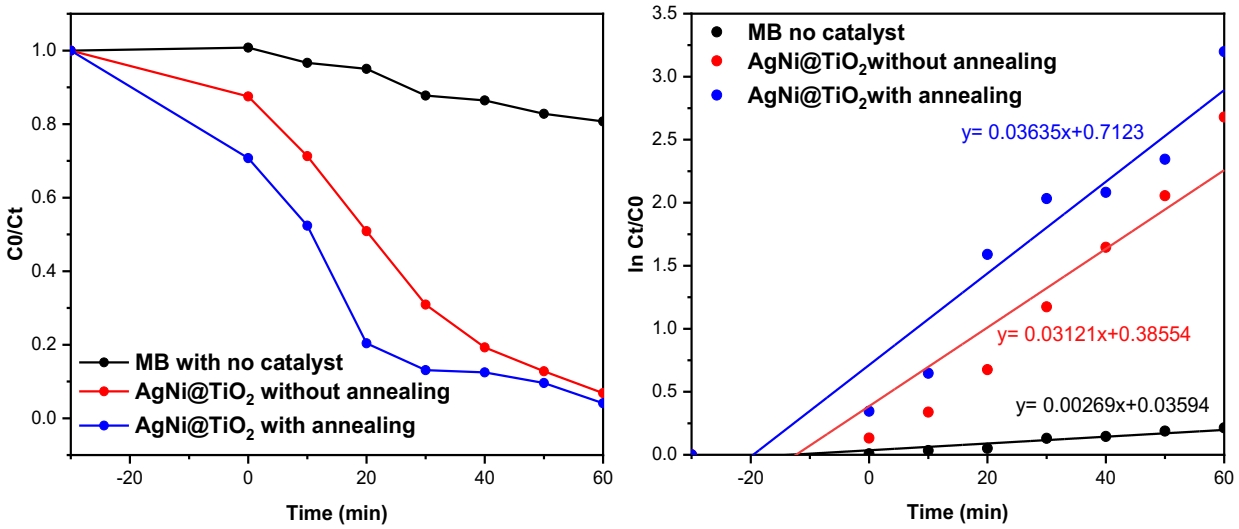


Figure 11. (a) Photocatalytic degrading of MB solution via the conventional $NiO/Ag/TiO_2$ catalyst (without annealing treatment), the composite with annealing treatment, and MB without catalyst in the presence of visible light for 60 minutes (b) Pseudo-first order kinetics of the decomposition of MB solution.

## 5.5 The $NiO/Ag/TiO_2$ Nanoparticles' Photocatalytic Degradation Mechanism Under the Influence of Visible Light.

The decolorization pathway depends on the degradation of the organic pollutant into non-toxic molecules such as $CO_2$, nitrate, ammonium, and sulfate ions by $OH^{\bullet}$ or $O2^{\bullet-}$ radicals regarding equations below (3-10).

$AgNi@TiO_2$+ visible light → $h^+$ (hole) + $e^-$ (electron) (3)

$h^+ + H_2O \rightarrow H^+ + OH^-$ (4)

$h^+ + OH- \rightarrow OH^\bullet$ (5)

$e^- + O_2 \rightarrow O_2^{\bullet-}$ (6)

$O_2^{\bullet-} + e^- + 2H^+ \rightarrow H_2O_2$ (7)

$O_2^{\bullet-} + H_2O_2 \rightarrow OH^\bullet + OH^- + O_2$ (8)

$OH^\bullet$ + organic compound → nontoxic products + $CO_2$↑ (9)

$O_2^{\bullet-}$ + organic compound → nontoxic products + $CO_2$↑ (10)

This method involved combining the semiconductor metal oxide $TiO_2$ with the metal oxide NiO and the metal Ag. The figure explains how radicals are created through the production of electron holes. NiO/Ag/$TiO_2$ has a unique combination that results in the formation of the metal and metal oxide interfaces, which creates a Schottky barrier.[109] The electrons can move from the valence band (VB) to the conduction band (CB) in visible light or from the VB to the mid-band gap transitions from the CB to Ti3+/Ov states, which are positioned below the CB, more quickly due to the $TiO_2$ NPs' relative ability to exciting the electrons. The charge carriers by holes for the NiO will switch from the VB of the $TiO_2$ to the VB of NiO. Dependably, the Ag NPs will behave as a photosensitizer and send more electrons to the CB of the $TiO_2$ which is linked with the NiO and $TiO_2$ surfaces. As a result of the p-n injection, these electrons may migrate to the CB of $TiO_2$ from the CB of NiO if the Ag NPs also transport electrons to the CB of NiO. The electrons will travel from NiO to $TiO_2$ downward as a consequence of the Schottky junction and the built-in electric field. This technique successfully prevented the electron hole from rapidly recombining, making more active electrons available for radical formation. Oxygen free radicals ($\bullet O^{2-}$) are produced as a result of the conduction band electrons being trapped by $O_2$ on hybrid shells. In the meantime, $H_2O$ or OH reacts with the holes in the valence band to form •OH (Figure 12). The MB dye

component will then decompose by the free radicals into a harmless substance and $CO_2$ gas as a byproduct.

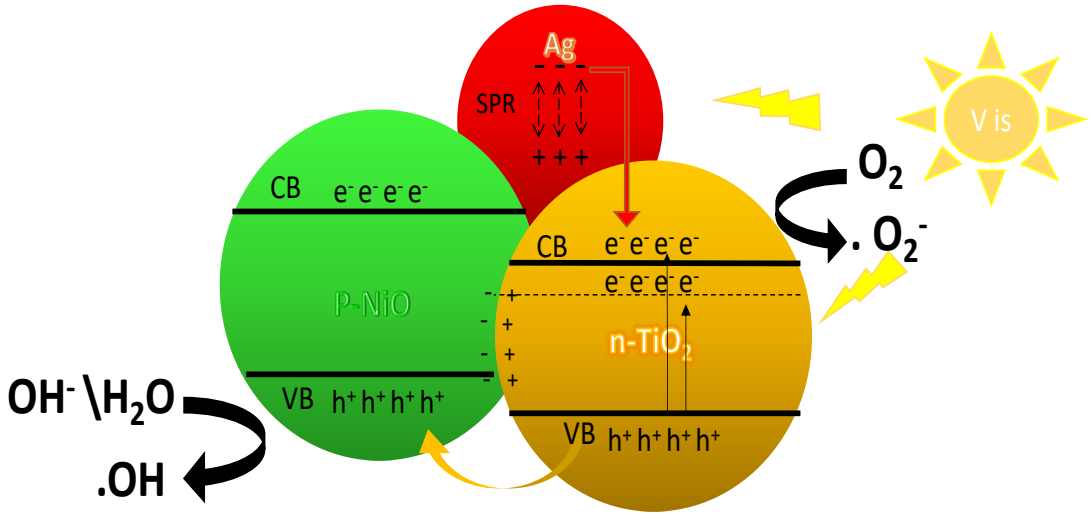


Figure 12. Mechanism of MB photodegradation reaction by NiO/Ag/$TiO_2$ composite when exposed to visible light.

5.6 Photocatalytic Degradation of Pharmaceutical Wastes (Aspirin and Paracetamol).

The NiO/Ag/$TiO_2$ nanocatalyst has been used to photodegrade medicines (paracetamol and aspirin). Various functional groups in the ASP and PCM provide the photocatalyst with a range of binding sites.[110] The two experiments have been done in identical conditions, NiO/Ag/$TiO_2$ ternary composites and $TiO_2$ as a reference, were used for the decomposition of both ASP and PCM by exposed visible light for 60 minutes. Figure 13 (a and b) show that NiO/Ag/$TiO_2$ has higher photocatalytic activity than bare TiO2 based on the results of the ASP and PCM. Within 60 minutes, the NiO/Ag/$TiO_2$ photocatalyst showed better degradation of the ASP and PCM than bare $TiO_2$ (77% and 68.4%, respectively). Therefore, the more binding sites there are on catalysts for the adsorption of therapeutic chemicals, the higher the photocatalytic activity will be. The irradiation of visible light forms

the hydroxyl and oxide radicals from $O_2$ and water absorbed on the surfaces of the photocatalysts, which leads to the formation of the electron-hole pairs. When these radicals oxidize medicinal ingredients, $CO_2$ and $H_2O$ are produced along with other byproducts.

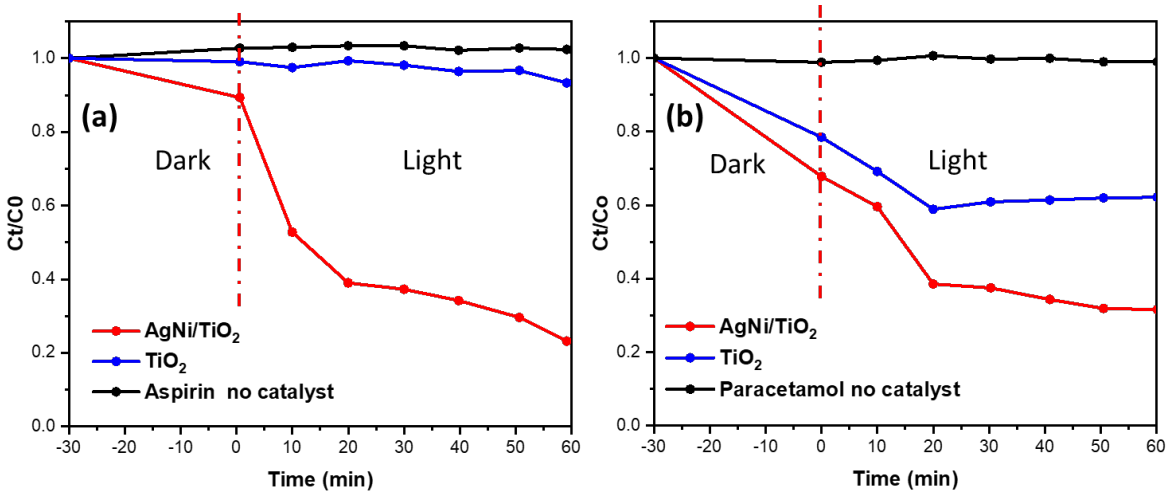


Figure 13. (a) The degradation of aspirin (b) and paracetamol beneath visible light for 60 minutes by NiO/Ag/$TiO_2$ and $TiO_2$ photocatalysts.

## 5.7 Recyclability

The 1% NiO/Ag/$TiO_2$ (1 g/L) photocatalytic activity experiment was conducted three times under similar conditions with the same photocatalyst being caught and dried each time to study the recyclability and photostability. According to Figure 14, the second and third cycles of the photocatalyst curves still exhibit close photocatalytic activity to that of the first cycle. However, the curve has slightly dropped to 90.4% in the third cycle. This study demonstrates that the 1% NiO/Ag/$TiO_2$ photocatalyst is stable, recyclable, and capable of degrading organic waste effectively.

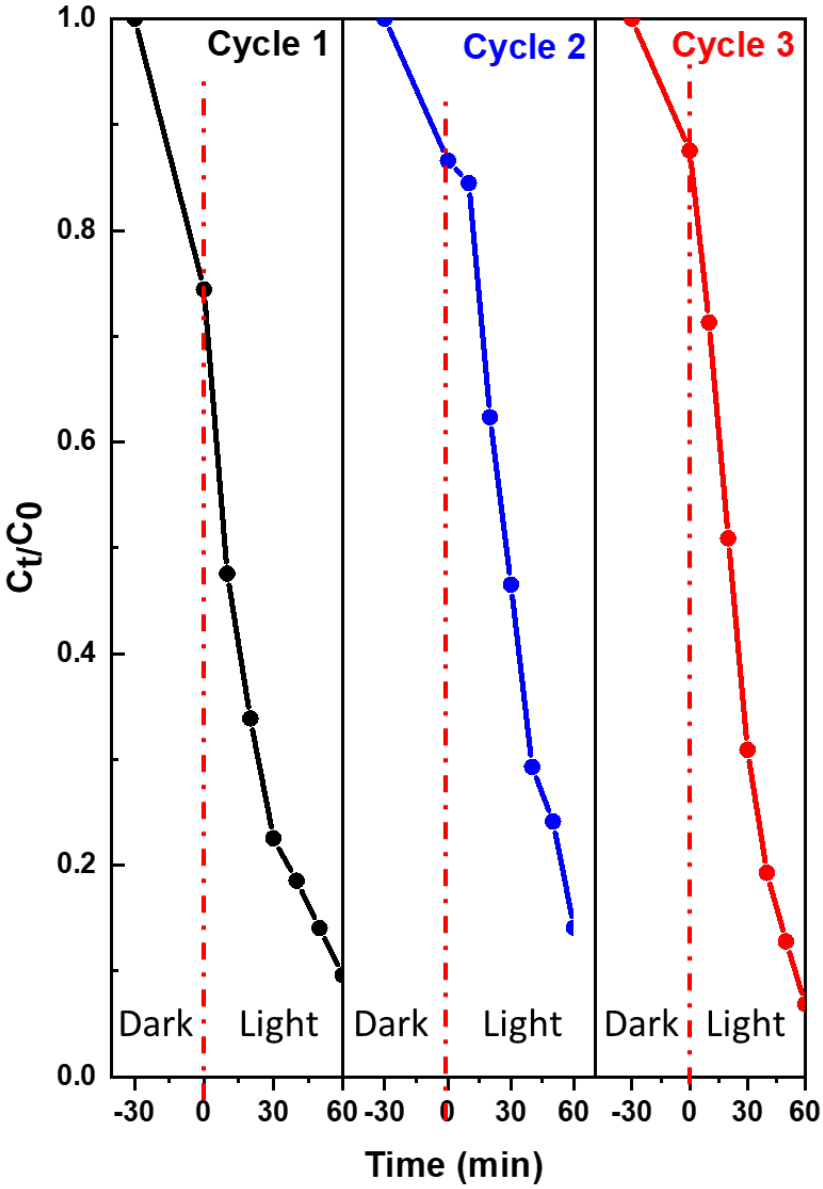


Figure 14. The performance of 1% NiO/Ag/$TiO_2$ photocatalyst of three cycles by measuring the decomposition of aqueous MB solution in the presence of visible light.

## 5.8 Antibacterial Activity

The anti-microbial activity of 1% NiO/Ag/$TiO_2$ nanocomposite on E. coli (Gram-negative) and S. aureus (Gram-positive) was investigated. Using a suspension test, the bactericidal property was examined for 1% NiO/Ag/$TiO_2$ in different irradiation conditions

(ambient light and dark). Figure 15(a-d) demonstrates the findings of the bactericidal and bacteriostatic effect of E. coli and S. aureus at various concentrations (0, 0.2, 0.5, and 1 g/L) of 1% NiO/Ag/$TiO_2$ in light and dark conditions.

Figure 15 illustrates that the 1% NiO/Ag/$TiO_2$ nanoparticles are dose-dependent in reducing bacteria growth when exposed to varying concentrations (0-1 g/L) of 1% NiO/Ag/$TiO_2$. As the amount of the nanoparticle's doses increases the inhibition of the bacteria growth increase in both light and dark conditions. According to Figure 14(a-d), it was found that E. coli (Gram-negative) represented more inhibition rate than S. aureus (Gram-positive). In addition, the 1g/L of 1% NiO/Ag/$TiO_2$ nanoparticle has a bactericidal effect on E. coli. However, Gram-negative bacteria have a cell membrane made up of a weak layer of peptidoglycan on the inside and a coating of liposaccharides on the outside[111]. The thin cell membrane of these bacteria makes them more vulnerable to silver ions that are produced from composite nanoparticles.[112] A previous study has found that Gram-positive bacteria are resistant to silver ions.[113] Due to a strong peptidoglycan layer consisting of teichoic acids in their cell membrane, which restricts the absorption of silver nanoparticles. [112]However, the reaction of each bacterium was determined by its metabolic properties.[113] Furthermore, another published paper illustrates that the Ag nanoparticles showed better inactivation of the Gram-negative bacteria than Gram-positive bacteria because of the electrostatic properties. Ag nanoparticles with a positive charge will attach easily to the Gram-negative bacteria with a negative charge membrane. [114]

Moreover, recent studies demonstrate that metal oxides such as ($TiO_2$, ZnO and Ni/$TiO_2$) have no effect on inhibiting the growth of bacteria in dark conditions. Also, metal oxides presented more inhibition for the cell wall of the Gram-positive bacteria.[115], [116] That can be concluded the addition of the silver nanoparticles in the Ni/$TiO_2$ not only

enhanced the killing and inactivation of the growth of Gram-negative bacteria but also improved the inhibiting of bacteria growth in the dark condition.

The antibacterial mechanism of $Ag^{+}$ and $Ag^{0}$ is partially known. However, several research claimed that the Ag NPs can cause major damage to the DNA by reacting with sulfur and phosphorus-containing compounds.[114] In addition, the production of reactive oxygen species (ROS) such as $O_2^{-}$, $H_2O_2$, and $OH^{\bullet}$ from the photocatalytic process can inhibit growth and kill the microorganisms by destroying the microorganism's cell wall.[117]–[119] Those theories can explain that the AgNi/$TiO_2$ nanocomposite can inhibit and kill all the microorganisms in light and dark conditions for a long time. Moreover, this disinfectant can be used as an antimicrobial spray for surfaces. However, it is important to know the cytotoxicity of this composite nanoparticle.

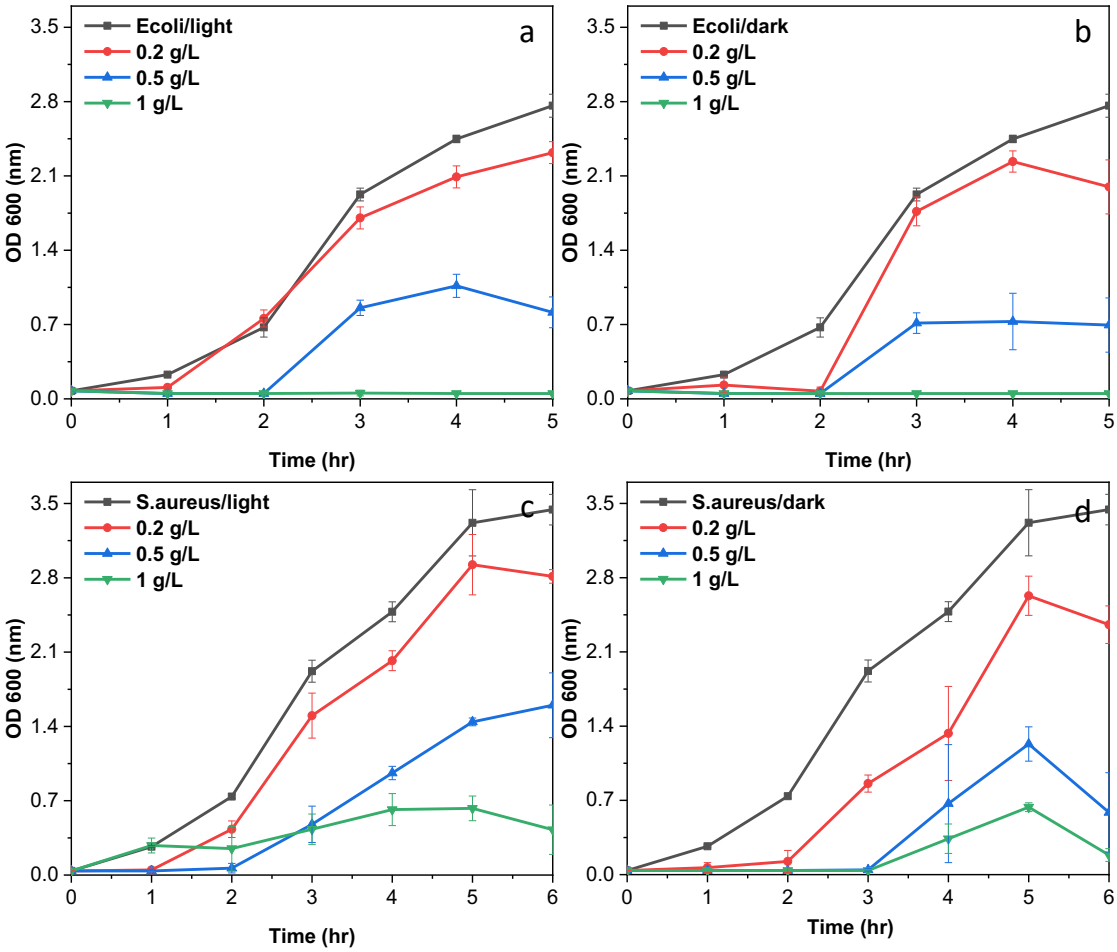


Figure 15. Dose-dependent inhibition of E. coli and S. aureus upon incubation at 37 °C with 1% NiO/Ag/$TiO_2$. (a) Bacterial growth of E. coli in the dark, (b) E. coli in light, (c) S. aureus in the dark, (d) and S. aureus in light, by adding different concentrations (0-1 g/L) of 1% NiO/Ag/$TiO_2$ as a function of the time for E. coli within 5 hours and S. aureus within 6 hours to reach the stationary phase.

# CHAPTER 6: SYNTHESIS AND CHARACTERIZATION OF VIRUS-LIKE MESOPOROUS SILICA NANOPARTICLES AND CYTOTOXICITY ASSESSMENT BY EMPLOYED ZEBRAFISH EMBRYOS.

## 6.1 Virus-like Mesopores Silica Nanoparticles Characterization

First, TEM and SEM techniques were used to describe the artificially created virus-like mesopores silica nanoparticles. The images in Figure 16 (a-e) show that the silica nanoparticles have evident short-length spikes (nanotubes) encircling the surface of the core-shell. This shape resembles that of a virus with a range in size from 125 to 168 nm for each nanoparticle. According to a recent study, by adjusting the CTAB concentration and speeding up the reaction time, the core-shell size of the V-MSN and the nanotube length may both be enhanced[24]. As a result, depending on the size of the drug, this feature will make it easier to insert any nonmedication by adjusting the two previous parameters.

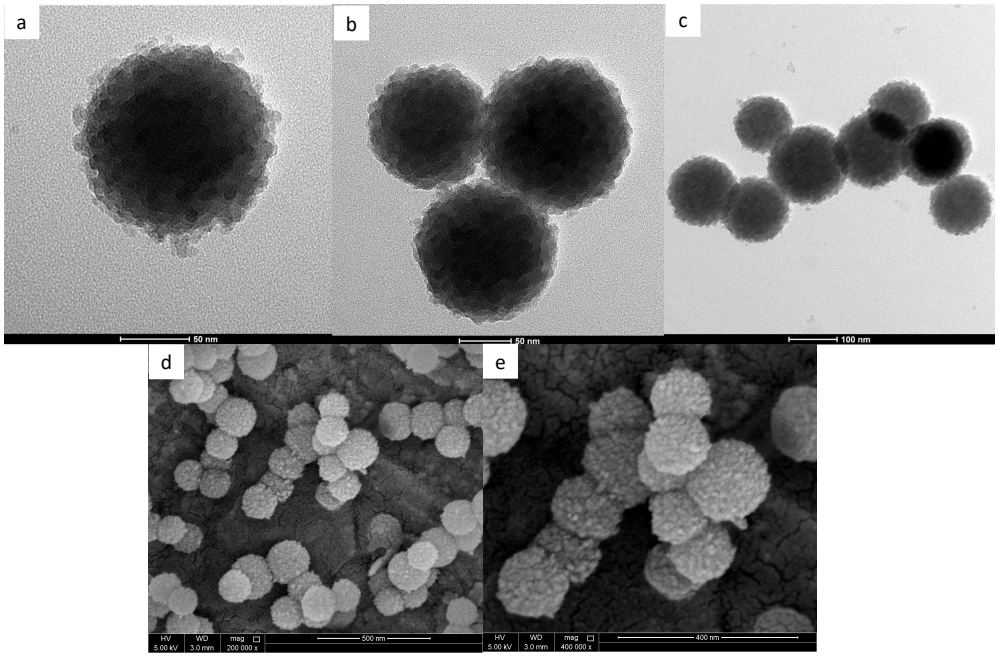


Figure 16. (a-c) The rough, virus-like interface of mesoporous silica nanoparticles is represented in TEM (d-e) and SEM images with various magnifications.

The surface area ($S_{BET}$) of virus-like mesoporous silica nanoparticles (V-MSN) and mesoporous silica nanoparticles was compared using the $N_2$ adsorption and desorption isotherm (MSN). The SBET for MSN is 84.754 $m^2/g$ and for V-MSN is 150.880 $m^2/g$, respectively, according to (Fig. 17a and b). Consequently, the addition of the spikes to the mesoporous silica nanoparticles' surfaces increased their surface area, which improved cellular endocytosis.[24] Additionally, as seen in, the pore size of V-MSN was 4 nm (Fig. 17c). The XRD pattern, which featured a single broad diffraction peak = 22.5 o, also showed that the VMSN followed amorphous morphologies (Fig. 17d).

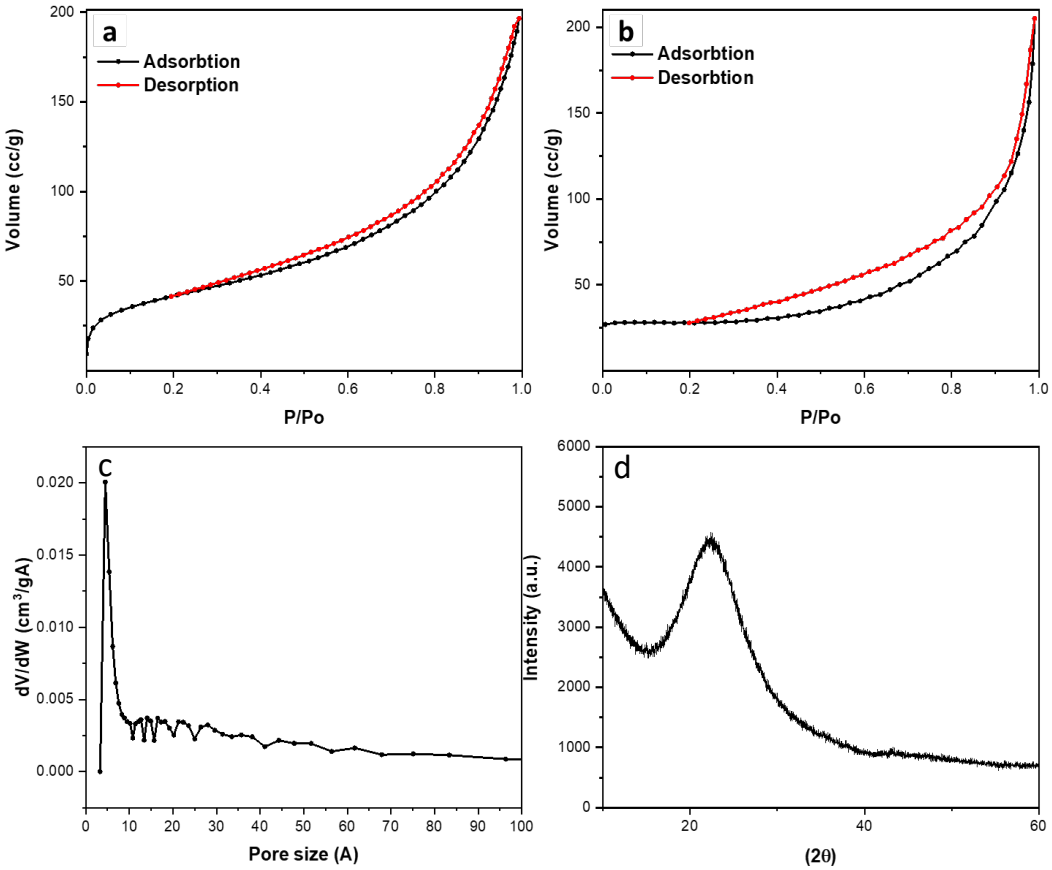


Figure 17. (a) Nitrogen adsorption isotherms of virus-like mesoporous silica nanoparticles (b) and mesoporous silica nanoparticles. (c)Pore size distribution (d) and XRD patterns of virus-like mesoporous silica nanoparticles.

## 6.2 Toxicity Assessment on Zebra Fish Embryos:

It is important to find the toxicity of the nanomaterial, especially that used in drug delivery which will involve the human body. Zebrafish embryos were used widely to evaluate their toxicity because they resemble those of mammals. In this investigation, different concentration of virus-like silica nanoparticles was used (200, 400, 600, 800, 1000, 1200, 1400, and 1600 mg/L) to detect the survival of zebrafish. PTU was used as negative control and (40 mg/L) of ZnO nanoparticles as a positive control. Previous work shows that the LOEC concentration (mortality value >20 %) for ZnO nanoparticles is 40 mg/L which a mortality value was 30% and the significant deformation in zebrafish (body abnormalities, heartbeat, movement, heart edema, and yolk edema embryos start to appear at the NOEC concentration (20 mg/L).[120]

At 96-hpf, the positive control ZnO nanoparticles represent 70% of the survival rate (14 of 20 embryos are life) as shown in Figure 18(a). For virus-like silica nanoparticles, a negligible ratio of mortality appeared at 600 mg/L (mortality rate <20%) which is considered NOEC. However, the ratio of the mortality starts to increase in the concentration of 800 mg/L of the drug which is a mortality rate of ~25% (LOEC). According to Figure 18(a), a dose-dependent rising in mortality can observe when the zebrafish embryos are exposed to the drug. Worthless, a negligible increase was observed in the survival rate of the embryos at 1200 mg/L, owing to the sedimentation of the nanoparticles when the medium is saturated. Therefore, by using the sigmoidal curve in Figure 18(b), the LC50 of ZnO and the virus-like silica nanoparticles were determined (51.91 and 1105 mg/L respectively). Hence, the tested drug can classify as non-hazard material upon the Fish and Wildlife Service's (FWS) scale for assessing acute toxicity.

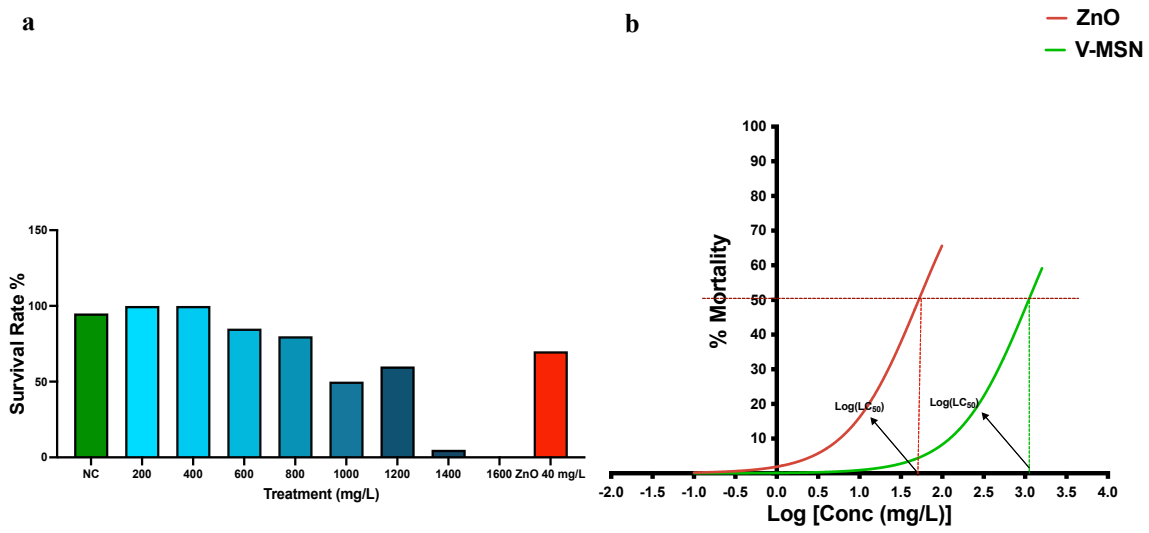


Figure 18. (a)The percentage of zebrafish embryos that survived after being incubated in PTU solution for 96 hpf (Negative Control, NC), after being exposed to 40 mg/L ZnO (Positive Control, PC), and 200, 400, 600, 800, 1000, 1200, 1400 and 1600 mg/L of virus-like mesoporous silica nanoparticles. (b) The mortality modeling curve for embryos treated with ZnO and virus-like mesoporous silica nanoparticles at various doses. The determined LC50 employing the sigmoidal curve for ZnO is 51.91, and for V-MSN is 1105 mg/L. 20 embryos were used for the experiment.

The next step is to prove that the nanoparticle is safe and won't result in teratogenic phenotypes or deformations in the zebrafish embryos. For this target, four areas were focused on which were: the body length, eye size, yolk sac size, and heart sac size to measure any abnormalities in the zebrafish embryos at 96-hbf. The embryo's body parts images are taken with the HCImage program and then the measurements are done with ImageJ software.

Figures 19 (a-f) show a random selection of zebrafish embryos that were treated with various concentrations (200-1000 mg/L) of the nanoparticles which does not represent any deformations compared to the NC. However, some of the zebrafish embryos that were exposed to 40 mg/L of ZnO nanoparticles (PC) for 96-hbf show an obvious distortion in eyes (small), heart sac size (edema), and yolk sac size (edema) as shown in Figure 19(e-g).

Furthermore, the average of zebrafish embryo measurements indicated a significant increase in the size of the heart when treated with the PC. In contrast, compared to the NC, there is no major change in the body length, eye, yolk sac, and heart sac sizes for the embryos that were treated with (200-1000 mg/L). However, a slight shrink in the heart sac and swelling in the yolk sac were reported in the embryos exposed to the 1200 mg/L Figure 20(a-d). To sum up, according to the investigations, virus-like silica mesopores nanoparticles are nontoxic and don't seriously endanger aquatic life up to 1000 mg/L.

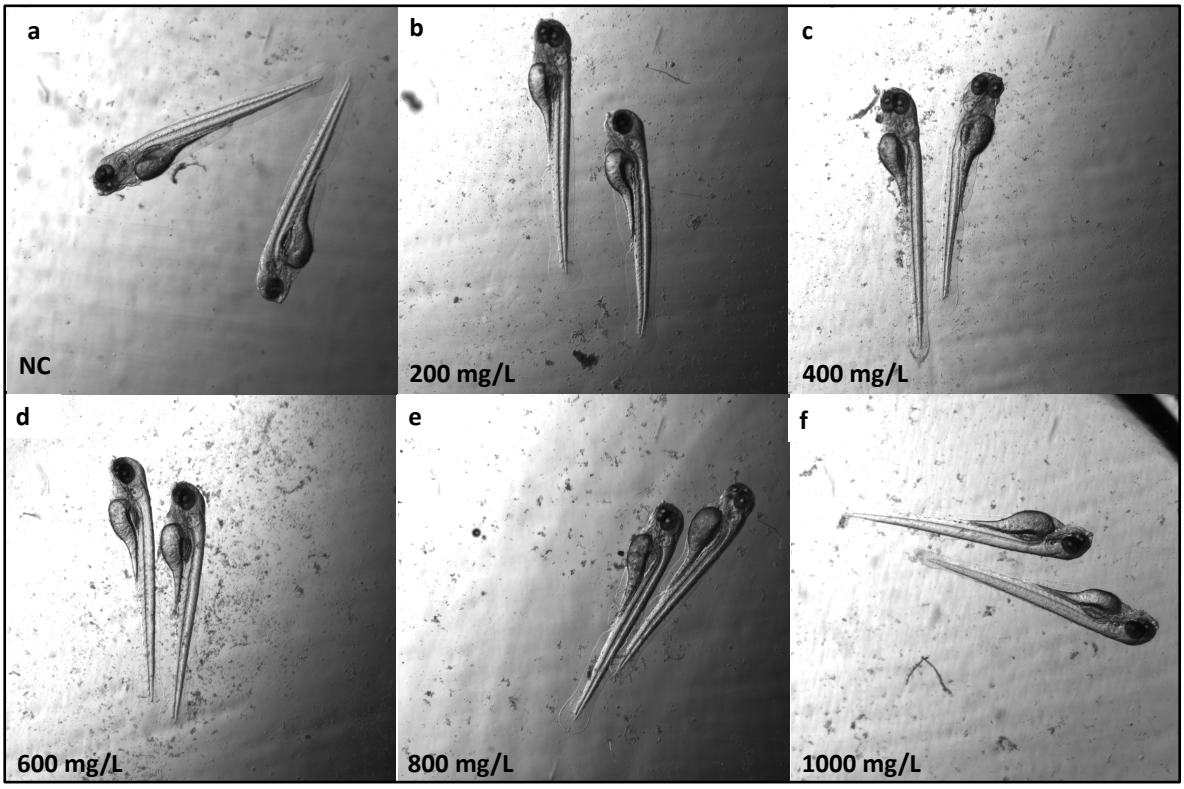


Figure 19. (a-f) Captured images using the HCImage program of a random selection of zebrafish embryos exposed to the nanoparticles with conc. of (0, 200, 400, 600, 800, and 1000 mg/L) to investigate any abnormalities in the body of the embryos.

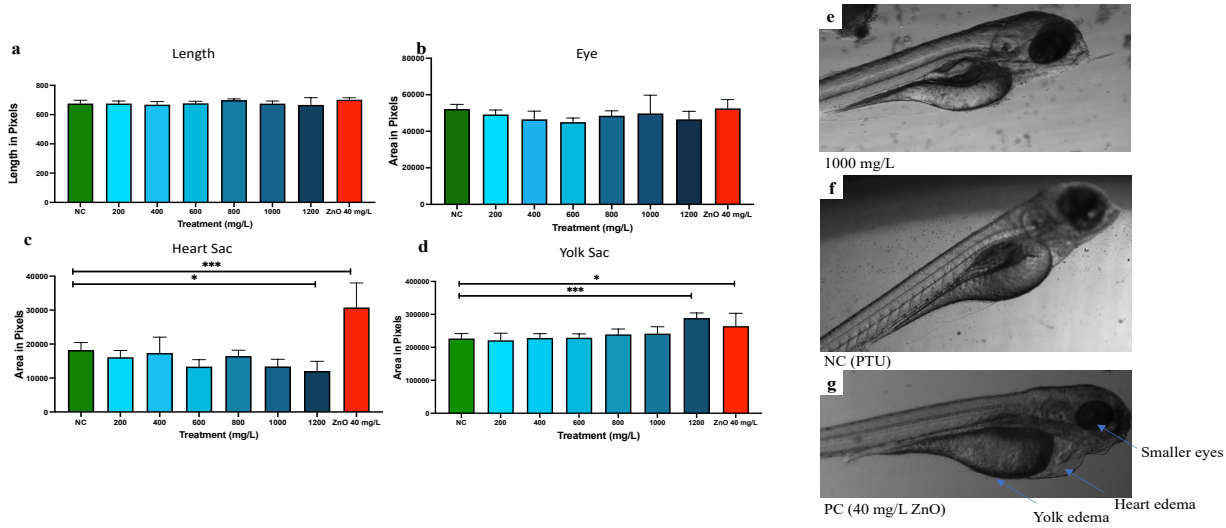


Figure 20. (a)The average measurements of body length embryos, (b) eye size, (c) heart sac size, (d) and yolk sac size were determined by utilizing the ImageJ program. (e-f) Captured images to show the deformations in the embryo that was treated with 40 mg/L compared to the NC and 1000 mg/L of V-MSN at 96-hpf. The variation between the average of the observed areas between groups was compared using a one-way analysis of variance (ANOVA), followed by the Dunnet testing. *p<0.05, **p<0.01, ***p<0.001.

# CHAPTER 7: CONCLUSION AND FUTURE WORK

In brief, the NiO/Ag/$TiO_2$ nanocomposite was successfully fabricated via a co-precipitation technique. The XRD, TEM, TEM-EDS mapping, HTEM, and XPS were utilized to characterize the synthesized sample. Hence, the Ag and Ni nanoparticles were uniformly dispersed with spherical shape with size (<10 nm) on the surface of the tetragonal rutile $TiO_2$ by a size range of (150-200 nm) with no other phase. In comparison to the other composites (1%Ag/$TiO_2$, 1%Ni/$TiO_2$, and bare $TiO_2$), the larger porosity and narrowing in the band gap caused the UV-absorption spectra to shift toward the red. Besides, the p-n-Schottky heterostructure within the nanocomposite structure caused to enhance the electron-hole pairs separation efficiency. All these factors are responsible for the improvement of the photocatalytic activity of the 1% NiO/Ag/$TiO_2$ by increasing the number of ROS. As a result, the highly stable and recyclable nanocomposite NiO/Ag/$TiO_2$ can function as an effective photocatalyst for the degradation of organic molecules, including pharmaceutical wastes (Aspirin and Paracetamol) and dyes (Methylene blue). The synthesized catalyst also exhibits an excellent disinfectant against bacteria of two types positive-gram and negative-gram under dark and light conditions. Furthermore, this material can be used to inhibit viruses, especially Covid-19. Further studies are required on the mechanisms of the deactivation of viruses. Also, it is crucial to study the toxicity of the 1% NiO/Ag/$TiO_2$ owing to the direct contact with the human as a disinfector. However, due to the high production of ROS, it can use in many other applications such as converting $CO_2$ to harmless products, water splitting, and cancer therapy.

On the other hand, the virus-like shape of silica mesoporous nanoparticles was also effectively produced in this work by using a dual micelle epitaxial growth method in an oil/water biphase reaction system with low surfactant concentration. Thus, this modification in the surface shape of the mesoporous led to developing the intracellular uptake as a drug

carrier. In this report, the cytotoxicity of the drug carrier was assessed via a zebrafish embryos model. As a result, the material does not show any toxicity up to 1000 mg/L which can conclude that the material is safe and non- hazard according to the Fish and Wildlife Service's (FWS) scale for evaluating acute toxicity. In future work, it can be loaded functional nanoparticles @VMSN core-shell using the same producing method, including a rough surface with mesopore channels and epitaxial spiky nanotubes that resemble a virus which makes an efficient in wide medical applications.

REFERENCE:


[1] S. Das, B. Sen, and N. Debnath, “Recent trends in nanomaterials applications in environmental monitoring and remediation,” *Environmental Science and Pollution Research*, vol. 22, no. 23, pp. 18333–18344, Dec. 2015, doi: 10.1007/S11356-015-5491-6/FIGURES/3.

[2] M. Shafiq, S. Anjum, C. Hano, I. Anjum, and B. H. Abbasi, “An Overview of the Applications of Nanomaterials and Nanodevices in the Food Industry,” *Foods 2020, Vol. 9, Page 148*, vol. 9, no. 2, p. 148, Feb. 2020, doi: 10.3390/FOODS9020148.

[3] A. C. V. Doughty, A. R. Hoover, E. Layton, C. K. Murray, E. W. Howard, and W. R. Chen, “Nanomaterial Applications in Photothermal Therapy for Cancer,” *Materials 2019, Vol. 12, Page 779*, vol. 12, no. 5, p. 779, Mar. 2019, doi: 10.3390/MA12050779.

[4] M. Iqbal, R. Khan, and N. Khan, “Salicylic Acid and Jasmonates: Approaches in Abiotic Stress Tolerance Article,” *J Plant Biochem Biotechnol*, 2013, doi: 10.4172/2329-9029.1000e113.

[5] S. Sur, A. Rathore, V. Dave, K. R. Reddy, R. S. Chouhan, and V. Sadhu, “Recent developments in functionalized polymer nanoparticles for efficient drug delivery system,” *Nano-Structures & Nano-Objects*, vol. 20, p. 100397, Oct. 2019, doi: 10.1016/J.NANOSO.2019.100397.

[6] A. Król, P. Pomastowski, K. Rafińska, V. Railean-Plugaru, and B. Buszewski, “Zinc oxide nanoparticles: Synthesis, antiseptic activity and toxicity mechanism,” *Adv Colloid Interface Sci*, vol. 249, pp. 37–52, Nov. 2017, doi: 10.1016/J.CIS.2017.07.033.

[7] V. Railean-Plugaru *et al.*, “Study of silver nanoparticles synthesized by acidophilic strain of Actinobacteria isolated from the of Picea sitchensis forest soil,” *J Appl Microbiol*, vol. 120, no. 5, pp. 1250–1263, May 2016, doi: 10.1111/JAM.13093.

[8] R. W. Kelsall, I. W. Hamley, and M. Geoghegan, “Nanoscale Science and

Technology," *Nanoscale Science and Technology*, pp. 1–456, Dec. 2005, doi: 10.1002/0470020873.

[9] J. Y. Song and B. S. Kim, "Biological synthesis of bimetallic Au/Ag nanoparticles using Persimmon (Diopyros kaki) leaf extract," *Korean Journal of Chemical Engineering 2008 25:4*, vol. 25, no. 4, pp. 808–811, Sep. 2008, doi: 10.1007/S11814-008-0133-Z.

[10] I. T. K and L. P. K, "Magnetic Nanoparticles – A Review," *International Journal of Pharmaceutical Sciences and Nanotechnology(IJPSN)*, vol. 3, no. 3, pp. 1035–1042, Nov. 2010, doi: 10.37285/IJPSN.2010.3.3.1.

[11] M. Delfi *et al.*, "Functionalization of Polymers and Nanomaterials for Biomedical Applications: Antimicrobial Platforms and Drug Carriers," *Prosthesis 2020, Vol. 2, Pages 117-139*, vol. 2, no. 2, pp. 117–139, Jun. 2020, doi: 10.3390/PROSTHESIS2020012.

[12] Q. Li *et al.*, "Antimicrobial nanomaterials for water disinfection and microbial control: Potential applications and implications," *Water Res*, vol. 42, no. 18, pp. 4591–4602, Nov. 2008, doi: 10.1016/J.WATRES.2008.08.015.

[13] P. Bhanja and A. Bhaumik, "Porous nanomaterials as green catalyst for the conversion of biomass to bioenergy," *Fuel*, vol. 185, pp. 432–441, Dec. 2016, doi: 10.1016/J.FUEL.2016.08.004.

[14] Y. Yang, S. Niu, D. Han, T. Liu, G. Wang, and Y. Li, "Progress in Developing Metal Oxide Nanomaterials for Photoelectrochemical Water Splitting," *Adv Energy Mater*, vol. 7, no. 19, p. 1700555, Oct. 2017, doi: 10.1002/AENM.201700555.

[15] M. Pumera, "Graphene-based nanomaterials for energy storage," *Energy Environ Sci*, vol. 4, no. 3, pp. 668–674, Mar. 2011, doi: 10.1039/C0EE00295J.

[16] J. Yao, M. Yang, and Y. Duan, "Chemistry, biology, and medicine of fluorescent

nanomaterials and related systems: New insights into biosensing, bioimaging, genomics, diagnostics, and therapy," *Chem Rev*, vol. 114, no. 12, pp. 6130–6178, Jun. 2014, doi: 10.1021/CR200359P/ASSET/IMAGES/LARGE/CR-2011-00359P_0002.JPEG.

[17] O. Akhavan, "Lasting antibacterial activities of Ag–TiO2/Ag/a-TiO2 nanocomposite thin film photocatalysts under solar light irradiation," *J Colloid Interface Sci*, vol. 336, no. 1, pp. 117–124, Aug. 2009, doi: 10.1016/J.JCIS.2009.03.018.

[18] M. Kumar and S. Deka, "Multiply Twinned AgNi Alloy Nanoparticles as Highly Active Catalyst for Multiple Reduction and Degradation Reactions," *ACS Appl Mater Interfaces*, vol. 6, no. 18, pp. 16071–16081, Sep. 2014, doi: 10.1021/AM503913Y.

[19] E. Grabowska, M. Marchelek, T. Klimczuk, W. Lisowski, and A. Zaleska-Medynska, "Preparation, characterization and photocatalytic activity of TiO2 microspheres decorated by bimetallic nanoparticles," *J Mol Catal A Chem*, vol. 424, pp. 241–253, Dec. 2016, doi: 10.1016/J.MOLCATA.2016.09.004.

[20] S. W. Verbruggen *et al.*, "Plasmonic gold–silver alloy on TiO2 photocatalysts with tunable visible light activity," *Appl Catal B*, vol. 156–157, pp. 116–121, Sep. 2014, doi: 10.1016/J.APCATB.2014.03.027.

[21] W. Wang *et al.*, "Facile Synthesis of Uniform Virus-like Mesoporous Silica Nanoparticles for Enhanced Cellular Internalization," *ACS Cent Sci*, vol. 3, no. 8, pp. 839–846, Aug. 2017, doi: 10.1021/ACSCENTSCI.7B00257.

[22] R. Sougrat *et al.*, "Electron Tomography of the Contact between T Cells and SIV/HIV-1: Implications for Viral Entry," *PLoS Pathog*, vol. 3, no. 5, p. e63, 2007, doi: 10.1371/JOURNAL.PPAT.0030063.

[23] B. Yang, Y. Chen, and J. Shi, "Mesoporous silica/organosilica nanoparticles: Synthesis, biological effect and biomedical application," *Materials Science and*

*Engineering R: Reports*, vol. 137, pp. 66–105, Jul. 2019, doi: 10.1016/J.MSER.2019.01.001.

[24] W. Wang *et al.*, "Facile Synthesis of Uniform Virus-like Mesoporous Silica Nanoparticles for Enhanced Cellular Internalization," *ACS Cent Sci*, vol. 3, no. 8, pp. 839–846, Aug. 2017, doi: 10.1021/ACSCENTSCI.7B00257/ASSET/IMAGES/LARGE/OC-2017-00257Q_0005.JPEG.

[25] J. Wisniak, "The History of Catalysis. From the Beginning to Nobel Prizes," *Educacion Quimica*, vol. 21, no. 1, pp. 60–69, Jan. 2010, doi: 10.1016/S0187-893X(18)30074-0.

[26] B. Lindström and L. J. Pettersson, "A Brief History of Catalysis," *CATTECH 2003 7:4*, vol. 7, no. 4, pp. 130–138, 2003, doi: 10.1023/A:1025001809516.

[27] "Chapter 1 History of catalysis," *Stud Surf Sci Catal*, vol. 79, no. C, pp. 3–21, Jan. 1993, doi: 10.1016/S0167-2991(08)63805-7.

[28] "Concepts of Modern Catalysis and Kinetics - J. W. Niemantsverdriet, I. Chorkendorff - كتبGoogle." https://books.google.com.qa/books?hl=ar&lr=&id=p34rVviEVWsC&oi=fnd&pg=PR7&dq=I.+Chorkendorff,+J.+W.+Niemantsverdriet,+Concepts+of+Modern+Catalysis+and+Kinetics,+John+Wiley+%26+Sons,+2003,+696+pp.&ots=gArWOKcogW&sig=eSqYGuyT17BYPyBqnhDspSP3fnU&redir_esc=y#v=onepage&q&f=false (accessed Sep. 27, 2022).

[29] D. Akademischer and A. Dienst, "DAAD MatCatNet-International Master and Postgraduate Programme in Material Science and Catalysis SCIENTIFIC AND METHODS MODULE Module name Catalysts Number 2013-MatCatNet02 Aims".

[30] "Effects of Catalyst Types and Concentrations on Biodiesel Production from Waste Soybean Oil Biomass as Renewable Energy and Environmental Recycling Process |

Australian Journal of Crop Science." https://search.informit.org/doi/epdf/10.3316/informit.536705085735213 (accessed Sep. 27, 2022).

[31] P. Chandra, Enespa, R. Singh, and P. K. Arora, "Microbial lipases and their industrial applications: a comprehensive review," *Microb Cell Fact*, vol. 19, no. 1, Aug. 2020, doi: 10.1186/S12934-020-01428-8.

[32] M. C. Román-Martínez and C. Salinas-Martínez de Lecea, "Heterogenization of Homogeneous Catalysts on Carbon Materials," *New and Future Developments in Catalysis: Hybrid Materials, Composites, and Organocatalysts*, pp. 55–78, 2013, doi: 10.1016/B978-0-444-53876-5.00003-9.

[33] S. M. George, "Introduction: Heterogeneous Catalysis," *Chem Rev*, vol. 95, no. 3, pp. 475–476, 1995, doi: 10.1021/CR00035A001/ASSET/CR00035A001.FP.PNG_V03.

[34] V. Kumar, T. Mohapatra, S. Dharmadhikari, and P. Ghosh, "A Review Paper on Heterogeneous Fenton Catalyst: Types of Preparation, Modification Techniques, Factors Affecting the Synthesis, Characterization, and Application in the Wastewater Treatment," *Bulletin of Chemical Reaction Engineering & Catalysis*, vol. 15, no. 1, pp. 1–34, Apr. 2020, doi: 10.9767/BCREC.15.1.4374.1-34.

[35] I. Khan, K. Saeed, and I. Khan, "Nanoparticles: Properties, applications and toxicities," *Arabian Journal of Chemistry*, vol. 12, no. 7, pp. 908–931, Nov. 2019, doi: 10.1016/J.ARABJC.2017.05.011.

[36] M. Mehta, M. Sharma, K. Pathania, P. K. Jena, and I. Bhushan, "Degradation of synthetic dyes using nanoparticles: a mini-review," *Environmental Science and Pollution Research*, vol. 28, no. 36, pp. 49434–49446, Sep. 2021, doi: 10.1007/S11356-021-15470-5/TABLES/3.

[37] "Introduction: Nanoparticles in Catalysis," 2020, doi: 10.1021/acs.chemrev.8b00696.

[38] M. Mehta, M. Sharma, K. Pathania, P. K. Jena, and I. Bhushan, "Degradation of synthetic dyes using nanoparticles: a mini-review," *Environmental Science and Pollution Research*, vol. 28, no. 36, pp. 49434–49446, Sep. 2021, doi: 10.1007/S11356-021-15470-5/TABLES/3.

[39] V. Kumar, T. Mohapatra, S. Dharmadhikari, and P. Ghosh, "A Review Paper on Heterogeneous Fenton Catalyst: Types of Preparation, Modification Techniques, Factors Affecting the Synthesis, Characterization, and Application in the Wastewater Treatment," *Bulletin of Chemical Reaction Engineering & Catalysis*, vol. 15, no. 1, pp. 1–34, Apr. 2020, doi: 10.9767/BCREC.15.1.4374.1-34.

[40] Y. M. Manawi, Ihsanullah, A. Samara, T. Al-Ansari, and M. A. Atieh, "A Review of Carbon Nanomaterials' Synthesis via the Chemical Vapor Deposition (CVD) Method," *Materials 2018, Vol. 11, Page 822*, vol. 11, no. 5, p. 822, May 2018, doi: 10.3390/MA11050822.

[41] I. Djerdj, A. M. Tonejc, M. Bijelić, V. Vraneša, and A. Turković, "Transmission electron microscopy studies of nanostructured TiO2 films on various substrates," *Vacuum*, vol. 80, no. 4, pp. 371–378, Oct. 2005, doi: 10.1016/J.VACUUM.2005.06.015.

[42] A. Kumar and G. Pandey, "Different Methods Used for the Synthesis of TiO 2 Based Nanomaterials: A Review," *American Journal of Nano Research and Applications*, vol. 6, no. 1, pp. 1–10, 2018, doi: 10.11648/j.nano.20180601.11.

[43] X. Li, X. Jin, N. Zhao, I. Angelidaki, and Y. Zhang, "Novel bio-electro-Fenton technology for azo dye wastewater treatment using microbial reverse-electrodialysis electrolysis cell," *Bioresour Technol*, vol. 228, pp. 322–329, Mar. 2017, doi: 10.1016/J.BIORTECH.2016.12.114.

[44] U. Shanker, M. Rani, and V. Jassal, "Degradation of hazardous organic dyes in water

by nanomaterials," *Environ Chem Lett*, vol. 15, no. 4, pp. 623–642, Dec. 2017, doi: 10.1007/S10311-017-0650-2.

[45] V. Katheresan, J. Kansedo, and S. Y. Lau, "Efficiency of various recent wastewater dye removal methods: A review," *J Environ Chem Eng*, vol. 6, no. 4, pp. 4676–4697, Aug. 2018, doi: 10.1016/J.JECE.2018.06.060.

[46] Y. Haldorai and J. J. Shim, "Chitosan-Zinc Oxide hybrid composite for enhanced dye degradation and antibacterial activity," *http://dx.doi.org/10.1080/15685543.2013.806124*, vol. 20, no. 5, pp. 365–377, Jul. 2013, doi: 10.1080/15685543.2013.806124.

[47] P. Rajasulochana and V. Preethy, "Comparison on efficiency of various techniques in treatment of waste and sewage water – A comprehensive review," *Resource-Efficient Technologies*, vol. 2, no. 4, pp. 175–184, Dec. 2016, doi: 10.1016/J.REFFIT.2016.09.004.

[48] Y. Deng and R. Zhao, "Advanced Oxidation Processes (AOPs) in Wastewater Treatment," *Curr Pollut Rep*, vol. 1, no. 3, pp. 167–176, Sep. 2015, doi: 10.1007/S40726-015-0015-Z/TABLES/2.

[49] R. Kaushik, P. K. Samal, and A. Halder, "Degradation of Fluoroquinolone-Based Pollutants and Bacterial Inactivation by Visible-Light-Active Aluminum-Doped TiO2 Nanoflakes," *ACS Appl Nano Mater*, vol. 2, no. 12, pp. 7898–7909, Dec. 2019, doi: 10.1021/ACSANM.9B01913/ASSET/IMAGES/LARGE/AN9B01913_0010.JPEG.

[50] V. Bhatia, A. Dhir, and S. K. Kansal, "Solar Light Induced Photocatalytic Degradation of Aspirin Using Doped TiO2 Nanoparticles," *J Nanosci Nanotechnol*, vol. 16, no. 7, pp. 7444–7450, Jul. 2016, doi: 10.1166/JNN.2016.11129.

[51] A. M. Abdel-Wahab, A. S. Al-Shirbini, O. Mohamed, and O. Nasr, "Photocatalytic degradation of paracetamol over magnetic flower-like TiO2/Fe2O3 core-shell

nanostructures," *J Photochem Photobiol A Chem*, vol. 347, pp. 186–198, Oct. 2017, doi: 10.1016/J.JPHOTOCHEM.2017.07.030.

[52] H. H. Lara, N. v. Ayala-Núñez, L. C. I. del Turrent, and C. R. Padilla, "Bactericidal effect of silver nanoparticles against multidrug-resistant bacteria," *World J Microbiol Biotechnol*, vol. 26, no. 4, pp. 615–621, Apr. 2010, doi: 10.1007/S11274-009-0211-3/FIGURES/3.

[53] A. A. Antsiferova, M. Y. Kopaeva, V. N. Kochkin, P. K. Kashkarov, and M. v Kovalchuk, "Accumulation of Silver Nanoparticles in Mice Brain Parts and the Harmful Effects," *J Nanomed Nanotechnol, an open access journal*, vol. 10, no. 1, p. 524, 2019, doi: 10.4172/2157-7439.1000524.

[54] T. Bruna, F. Maldonado-Bravo, P. Jara, and N. Caro, "Silver Nanoparticles and Their Antibacterial Applications," *Int J Mol Sci*, vol. 22, no. 13, Jul. 2021, doi: 10.3390/IJMS22137202.

[55] M. K. Rai, S. D. Deshmukh, A. P. Ingle, and A. K. Gade, "Silver nanoparticles: the powerful nanoweapon against multidrug-resistant bacteria," *J Appl Microbiol*, vol. 112, no. 5, pp. 841–852, May 2012, doi: 10.1111/J.1365-2672.2012.05253.X.

[56] S. W. Kim, J. H. Jung, K. Lamsal, Y. S. Kim, J. S. Min, and Y. S. Lee, "Antifungal Effects of Silver Nanoparticles (AgNPs) against Various Plant Pathogenic Fungi," *Mycobiology*, vol. 40, no. 1, p. 53, Mar. 2012, doi: 10.5941/MYCO.2012.40.1.053.

[57] D. Franco, G. Calabrese, S. P. P. Guglielmino, and S. Conoci, "Metal-Based Nanoparticles: Antibacterial Mechanisms and Biomedical Application," *Microorganisms 2022, Vol. 10, Page 1778*, vol. 10, no. 9, p. 1778, Sep. 2022, doi: 10.3390/MICROORGANISMS10091778.

[58] M. Natan, O. Gutman, R. Lavi, S. Margel, and E. Banin, "Killing mechanism of stable N-halamine cross-linked polymethacrylamide nanoparticles that selectively target

bacteria," *ACS Nano*, vol. 9, no. 2, pp. 1175–1188, Feb. 2015, doi: 10.1021/NN507168X/SUPPL_FILE/NN507168X_SI_001.PDF.

[59] H. M. Yadav, J. S. Kim, and S. H. Pawar, "Developments in photocatalytic antibacterial activity of nano TiO2: A review," *Korean Journal of Chemical Engineering 2016 33:7*, vol. 33, no. 7, pp. 1989–1998, Jun. 2016, doi: 10.1007/S11814-016-0118-2.

[60] Q. Li *et al.*, "Antimicrobial nanomaterials for water disinfection and microbial control: Potential applications and implications," *Water Res*, vol. 42, no. 18, pp. 4591–4602, Nov. 2008, doi: 10.1016/J.WATRES.2008.08.015.

[61] A. Król, P. Pomastowski, K. Rafińska, V. Railean-Plugaru, and B. Buszewski, "Zinc oxide nanoparticles: Synthesis, antiseptic activity and toxicity mechanism," *Adv Colloid Interface Sci*, vol. 249, pp. 37–52, Nov. 2017, doi: 10.1016/J.CIS.2017.07.033.

[62] Q. Li *et al.*, "Antimicrobial nanomaterials for water disinfection and microbial control: Potential applications and implications," *Water Res*, vol. 42, no. 18, pp. 4591–4602, Nov. 2008, doi: 10.1016/J.WATRES.2008.08.015.

[63] S. Agnihotri, D. Sillu, G. Sharma, and R. K. Arya, "Photocatalytic and antibacterial potential of silver nanoparticles derived from pineapple waste: process optimization and modeling kinetics for dye removal," *Appl Nanosci*, vol. 8, no. 8, pp. 2077–2092, Nov. 2018, doi: 10.1007/S13204-018-0883-9.

[64] W. Choi, A. Termin, and M. R. Hoffmann, "The role of metal ion dopants in quantum-sized TiO2: Correlation between photoreactivity and charge carrier recombination dynamics," *Journal of Physical Chemistry*, vol. 98, no. 51, pp. 13669–13679, 1994, doi: 10.1021/J100102A038/ASSET/J100102A038.FP.PNG_V03.

[65] H. M. Yadav, J.-S. Kim, and S. Hariba Pawar, "Developments in photocatalytic antibacterial activity of nano TiO 2 : A review," *Korean J. Chem. Eng*, vol. 33, no. 7,

pp. 1989–1998, 2016, doi: 10.1007/s11814-016-0118-2.

[66] M. H. Geesi, O. Ouerghi, A. Elsanousi, A. Kaiba, and Y. Riadi, "Ultrasound-Assisted Preparation of Cu-Doped TiO2 Nanoparticles as a Nanocatalyst for Sonochemical Synthesis of Pyridopyrimidines," *https://doi.org/10.1080/10406638.2020.1716029*, vol. 42, no. 1, pp. 80–90, 2020, doi: 10.1080/10406638.2020.1716029.

[67] Y. Mingmongkol *et al.*, "Enhanced Photocatalytic and Photokilling Activities of Cu-Doped TiO2 Nanoparticles," *Nanomaterials*, vol. 12, no. 7, Apr. 2022, doi: 10.3390/NANO12071198.

[68] B. Choudhury, M. Dey, and A. Choudhury, "Defect generation, d-d transition, and band gap reduction in Cu-doped TiO2 nanoparticles," *International Nano Letters 2013 3:1*, vol. 3, no. 1, pp. 1–8, Apr. 2013, doi: 10.1186/2228-5326-3-25.

[69] C. Karunakaran, G. Abiramasundari, P. Gomathisankar, G. Manikandan, and V. Anandi, "Cu-doped TiO(2) nanoparticles for photocatalytic disinfection of bacteria under visible light," *J Colloid Interface Sci*, vol. 352, no. 1, pp. 68–74, Dec. 2010, doi: 10.1016/J.JCIS.2010.08.012.

[70] A. B. Aritonang, E. Pratiwi, W. Warsidah, S. I. Nurdiansyah, and R. Risko, "Fe-doped TiO2/Kaolinite as an Antibacterial Photocatalyst under Visible Light Irradiation," *Bulletin of Chemical Reaction Engineering & Catalysis*, vol. 16, no. 2, pp. 293–301, Jun. 2021, doi: 10.9767/BCREC.16.2.10325.293-301.

[71] J. Ananpattarachai, Y. Boonto, and P. Kajitvichyanukul, "Visible light photocatalytic antibacterial activity of Ni-doped and N-doped TiO2 on Staphylococcus aureus and Escherichia coli bacteria," *Environ Sci Pollut Res Int*, vol. 23, no. 5, pp. 4111–4119, Mar. 2016, doi: 10.1007/S11356-015-4775-1.

[72] S. M. Gupta and M. Tripathi, "A review of TiO2 nanoparticles," *Chinese Science Bulletin 2011 56:16*, vol. 56, no. 16, pp. 1639–1657, May 2011, doi: 10.1007/S11434-

011-4476-1.

[73] L. Caballero, K. A. Whitehead, N. S. Allen, and J. Verran, “Photocatalytic inactivation of Escherichia coli using doped titanium dioxide under fluorescent irradiation,” *J Photochem Photobiol A Chem*, vol. 276, pp. 50–57, Feb. 2014, doi: 10.1016/J.JPHOTOCHEM.2013.11.017.

[74] C. L. Cheng *et al.*, “The effects of the bacterial interaction with visible-light responsive titania photocatalyst on the bactericidal performance,” *J Biomed Sci*, vol. 16, no. 1, pp. 1–10, Jan. 2009, doi: 10.1186/1423-0127-16-7/FIGURES/5.

[75] V. Etacheri, G. Michlits, M. K. Seery, S. J. Hinder, and S. C. Pillai, “A highly efficient TiO(2-x)C(x) nano-heterojunction photocatalyst for visible light induced antibacterial applications,” *ACS Appl Mater Interfaces*, vol. 5, no. 5, pp. 1663–1672, Mar. 2013, doi: 10.1021/AM302676A.

[76] G. A. Hughes, “Nanostructure-mediated drug delivery,” *Nanomedicine*, vol. 1, no. 1, pp. 22–30, Mar. 2005, doi: 10.1016/J.NANO.2004.11.009.

[77] E. Aznar, E. Climent, L. Mondragon, F. Sancenón, and R. Martínez-Máñez, “Functionalized Mesoporous Materials with Gate-Like Scaffoldings for Controlled Delivery,” *Polymers in Regenerative Medicine: Biomedical Applications from Nano- to Macro-Structures*, pp. 337–366, Jan. 2014, doi: 10.1002/9781118356692.CH10.

[78] E. Che *et al.*, “Paclitaxel/gelatin coated magnetic mesoporous silica nanoparticles: Preparation and antitumor efficacy in vivo,” *Microporous and Mesoporous Materials*, vol. C, no. 204, pp. 226–234, Mar. 2015, doi: 10.1016/J.MICROMESO.2014.11.013.

[79] C. Bharti, U. Nagaich, A. K. Pal, and N. Gulati, “Mesoporous silica nanoparticles in target drug delivery system: A review,” *Int J Pharm Investig*, vol. 5, no. 3, p. 124, 2015, doi: 10.4103/2230-973X.160844.

[80] C. Bharti, U. Nagaich, A. K. Pal, and N. Gulati, “Mesoporous silica nanoparticles in

target drug delivery system: A review," *Int J Pharm Investig*, vol. 5, no. 3, p. 124, 2015, doi: 10.4103/2230-973X.160844.

[81] "Synthesis of mesoporous SiO2 nanoparticles and toxicity assessment in early life stages of zebrafish," *Microporous and Mesoporous Materials*, vol. 330, p. 111573, Jan. 2022, doi: 10.1016/J.MICROMESO.2021.111573.

[82] M. Ahola, P. Kortesuo, I. Kangasniemi, J. Kiesvaara, and A. Yli-Urpo, "Silica xerogel carrier material for controlled release of toremifene citrate," *Int J Pharm*, vol. 195, no. 1–2, pp. 219–227, Feb. 2000, doi: 10.1016/S0378-5173(99)00403-2.

[83] C. Bharti, N. Gulati, U. Nagaich, and A. Pal, "Mesoporous silica nanoparticles in target drug delivery system: A review," *Int J Pharm Investig*, vol. 5, no. 3, p. 124, 2015, doi: 10.4103/2230-973X.160844.

[84] C. J. Brinker, "Porous inorganic materials," *Curr Opin Solid State Mater Sci*, vol. 1, no. 6, pp. 798–805, Dec. 1996, doi: 10.1016/S1359-0286(96)80104-5.

[85] A. Firouzi *et al.*, "Cooperative Organization of Inorganic-Surfactant and Biomimetic Assemblies," *Science (1979)*, vol. 267, no. 5201, pp. 1138–1143, Feb. 1995, doi: 10.1126/SCIENCE.7855591.

[86] M. A. Shahbazi, B. Herranz, and H. A. Santos, "Nanostructured porous Si-based nanoparticles for targeted drug delivery," *https://doi.org/10.4161/biom.22347*, vol. 2, no. 4, pp. 296–312, 2012, doi: 10.4161/BIOM.22347.

[87] M. Vallet-Regí, I. Izquierdo-Barba, and M. Colilla, "Structure and functionalization of mesoporous bioceramics for bone tissue regeneration and local drug delivery," *Philos Trans A Math Phys Eng Sci*, vol. 370, no. 1963, pp. 1400–1421, Mar. 2012, doi: 10.1098/RSTA.2011.0258.

[88] D. Halamová and V. Zeleňák, "NSAID naproxen in mesoporous matrix MCM-41: Drug uptake and release properties," *J Incl Phenom Macrocycl Chem*, vol. 72, no. 1–

2, pp. 15–23, Feb. 2012, doi: 10.1007/S10847-011-9990-X.

[89] F. Balas, M. Manzano, P. Horcajada, and M. Vallet-Regi, "Confinement and controlled release of bisphosphonates on ordered mesoporous silica-based materials," *J Am Chem Soc*, vol. 128, no. 25, pp. 8116–8117, Jun. 2006, doi: 10.1021/JA062286Z/SUPPL_FILE/JA062286ZSI20060404_072611.PDF.

[90] H. Du, P. D. Hamilton, M. A. Reilly, A. d'Avignon, P. Biswas, and N. Ravi, "A facile synthesis of highly water-soluble, core–shell organo-silica nanoparticles with controllable size via sol–gel process," *J Colloid Interface Sci*, vol. 340, no. 2, pp. 202–208, Dec. 2009, doi: 10.1016/J.JCIS.2009.08.032.

[91] L. Bergman *et al.*, "Intracellular degradation of multilabeled poly(ethylene imine)-mesoporous silica-silica nanoparticles: implications for drug release," *Mol Pharm*, vol. 10, no. 5, pp. 1795–1803, May 2013, doi: 10.1021/MP3005879.

[92] J. Zhang *et al.*, "Multifunctional envelope-type mesoporous silica nanoparticles for tumor-triggered targeting drug delivery," *J Am Chem Soc*, vol. 135, no. 13, pp. 5068–5073, Apr. 2013, doi: 10.1021/JA312004M.

[93] M. Colilla, I. Izquierdo-Barba, and M. Vallet-Regí, "Phosphorus-containing SBA-15 materials as bisphosphonate carriers for osteoporosis treatment," *Microporous and Mesoporous Materials*, vol. 135, no. 1–3, pp. 51–59, 2010, doi: 10.1016/J.MICROMESO.2010.06.010.

[94] C. Y. Lai *et al.*, "A mesoporous silica nanosphere-based carrier system with chemically removable CdS nanoparticle caps for stimuli-responsive controlled release of neurotransmitters and drug molecules," *J Am Chem Soc*, vol. 125, no. 15, pp. 4451–4459, Apr. 2003, doi: 10.1021/JA028650L/SUPPL_FILE/JA028650LSI20030120_115112.PDF.

[95] Z. Liu *et al.*, "Uniform dendrimer-like mesoporous silica nanoparticles as a nano-

adjuvant for foot-and-mouth disease virus-like particle vaccine," *J Mater Chem B*, vol. 7, no. 21, pp. 3446–3454, May 2019, doi: 10.1039/C8TB03315C.

[96] P. Wang *et al.*, "Virus-like mesoporous silica-coated plasmonic Ag nanocube with strong bacteria adhesion for diabetic wound ulcer healing," *Nanomedicine*, vol. 34, p. 102381, Jun. 2021, doi: 10.1016/J.NANO.2021.102381.

[97] S. M. Häffner *et al.*, "Membrane Interactions of Virus-like Mesoporous Silica Nanoparticles," *ACS Nano*, vol. 15, no. 4, pp. 6787–6800, Apr. 2021, doi: 10.1021/ACSNANO.0C10378/ASSET/IMAGES/LARGE/NN0C10378_0008.JPEG.

[98] G. J. Lieschke and P. D. Currie, "Animal models of human disease: zebrafish swim into view," *Nature Reviews Genetics 2007 8:5*, vol. 8, no. 5, pp. 353–367, May 2007, doi: 10.1038/nrg2091.

[99] M. B. Veldman and S. Lin, "Zebrafish as a Developmental Model Organism for Pediatric Research," *Pediatric Research 2008 64:5*, vol. 64, no. 5, pp. 470–476, Nov. 2008, doi: 10.1203/pdr.0b013e318186e609.

[100] G. K. Nasrallah *et al.*, "A systematic investigation of the bio-toxicity of core-shell magnetic mesoporous silica microspheres using zebrafish model," *Microporous and Mesoporous Materials*, vol. 265, pp. 195–201, Jul. 2018, doi: 10.1016/J.MICROMESO.2018.02.008.

[101] K. Saoud, R. al Soubaihi, S. Saeed, N. Bensalah, M. Al-Fandi, and T. Singh, "Heterogeneous Ag and ZnOBased Photocatalytic ForWaste Water Treatment Under Different Irradiation Conditions," *J. Mater. Environ. Sci*, vol. 9, no. 2, pp. 400–413, 2018, doi: 10.26872/jmes.2018.9.2.44.

[102] S. Liu, H. Sun, A. Suvorova, and S. Wang, "One-pot hydrothermal synthesis of ZnO-reduced graphene oxide composites using Zn powders for enhanced photocatalysis," *Chemical Engineering Journal*, vol. 229, pp. 533–539, Aug. 2013, doi:

10.1016/J.CEJ.2013.06.063.

[103] M. Matalkeh *et al.*, "Visible Light Photocatalytic Activity of Ag/WO3 Nanoparticles and its Antibacterial Activity Under Ambient Light and in The Dark," *Results in Engineering*, vol. 13, Mar. 2022, doi: 10.1016/j.rineng.2021.100313.

[104] S. Sankar and K. G. Gopchandran, "Effect of annealing on the structural, electrical and optical properties of nanostructured TiO2 thin films," *Crystal Research and Technology*, vol. 44, no. 9, pp. 989–994, Sep. 2009, doi: 10.1002/CRAT.200900073.

[105] S. Sugapriya, R. Sriram, and S. Lakshmi, "Effect of annealing on TiO2 nanoparticles," *Optik (Stuttg)*, vol. 124, no. 21, pp. 4971–4975, Nov. 2013, doi: 10.1016/J.IJLEO.2013.03.040.

[106] K. Kusdianto, D. Jiang, M. Kubo, and M. Shimada, "Effect of annealing temperature on the photocatalytic activity of Ag-TiO 2 nanocomposite films by one-step gas-phase deposition," 2017, doi: 10.1016/j.materresbull.2017.08.062.

[107] C. P. Lin, H. Chen, A. Nakaruk, P. Koshy, and C. C. Sorrell, "Effect of Annealing Temperature on the Photocatalytic Activity of TiO2 Thin Films," *Energy Procedia*, vol. 34, pp. 627–636, Jan. 2013, doi: 10.1016/J.EGYPRO.2013.06.794.

[108] V. S. K. Chakravadhanula *et al.*, "Surface segregation in TiO2-based nanocomposite thin films," *Nanotechnology*, vol. 23, no. 49, Dec. 2012, doi: 10.1088/0957-4484/23/49/495701.

[109] "Tuning of metal oxides photocatalytic performance using Ag nanoparticles integration | Elsevier Enhanced Reader." https://reader.elsevier.com/reader/sd/pii/S016773222030653X?token=9701BC9EF38AD7019DCCB2BB06FD365AC104A5D34E50B328E38366DBFBD2EE9B5EF2B44F2051FAD27BB8F9B5EB188A07&originRegion=eu-west-1&originCreation=20211226072551 (accessed Dec. 26, 2021).

[110] S. Bhardwaj and B. Pal, “Role of different oxidation states of Crn+-TiO2 nanocomposites for the degradation of drugs under solar irradiation,” *Mater Chem Phys*, vol. 269, Sep. 2021, doi: 10.1016/j.matchemphys.2021.124740.

[111] L. Misba, S. Zaidi, and A. U. Khan, “A comparison of antibacterial and antibiofilm efficacy of phenothiazinium dyes between Gram positive and Gram negative bacterial biofilm,” *Photodiagnosis Photodyn Ther*, vol. 18, pp. 24–33, Jun. 2017, doi: 10.1016/J.PDPDT.2017.01.177.

[112] K. J. Woo, C. K. Hye, W. K. Ki, S. Shin, H. K. So, and H. P. Yong, “Antibacterial activity and mechanism of action of the silver ion in Staphylococcus aureus and Escherichia coli,” *Appl Environ Microbiol*, vol. 74, no. 7, pp. 2171–2178, Apr. 2008, doi: 10.1128/AEM.02001-07.

[113] E. Pazos-Ortiz *et al.*, “Dose-Dependent Antimicrobial Activity of Silver Nanoparticles on Polycaprolactone Fibers against Gram-Positive and Gram-Negative Bacteria,” *J Nanomater*, vol. 2017, 2017, doi: 10.1155/2017/4752314.

[114] M. Guzman, J. Dille, and S. Godet, “Synthesis and antibacterial activity of silver nanoparticles against gram-positive and gram-negative bacteria,” *Nanomedicine: Nanotechnology, Biology, and Medicine*, vol. 8, no. 1. pp. 37–45, Jan. 2012. doi: 10.1016/j.nano.2011.05.007.

[115] A. Azam, A. S. Ahmed, M. Oves, M. S. Khan, S. S. Habib, and A. Memic, “Antimicrobial activity of metal oxide nanoparticles against Gram-positive and Gram-negative bacteria: A comparative study,” *Int J Nanomedicine*, vol. 7, pp. 6003–6009, 2012, doi: 10.2147/IJN.S35347.

[116] “Synthesis and visible light photocatalytic antibacterial activity of nickel-doped TiO2 nanoparticles against Gram-positive and Gram-negative bacteria | Elsevier Enhanced Reader.”

https://reader.elsevier.com/reader/sd/pii/S1010603014003359?token=5DC1EFBFF8D24A95D37DEA9F4FDB065B99296D73C7E7B811C79BF98C818303ABAAA65E125268DF35730D3CD30CC04E5C&originRegion=eu-west-1&originCreation=20211208060325 (accessed Dec. 08, 2021).

[117] G. Yang *et al.*, "Synergistic Ag/TiO2-N photocatalytic system and its enhanced antibacterial activity towards Acinetobacter baumannii," *Appl Catal B*, vol. 224, pp. 175–182, May 2018, doi: 10.1016/j.apcatb.2017.10.052.

[118] O. Akhavan, "Lasting antibacterial activities of Ag-TiO2/Ag/a-TiO2 nanocomposite thin film photocatalysts under solar light irradiation," *J Colloid Interface Sci*, vol. 336, no. 1, pp. 117–124, Aug. 2009, doi: 10.1016/j.jcis.2009.03.018.

[119] P. C. Maness, S. Smolinski, D. M. Blake, Z. Huang, E. J. Wolfrum, and W. A. Jacoby, "Bactericidal activity of photocatalytic TiO2 reaction: Toward an understanding of its killing mechanism," *Appl Environ Microbiol*, vol. 65, no. 9, pp. 4094–4098, 1999, doi: 10.1128/AEM.65.9.4094-4098.1999/ASSET/65CB98B3-C968-4BB7-B1EC-9CA3292DBBA9/ASSETS/GRAPHIC/AM0990169003.JPEG.

[120] G. K. Nasrallah, R. Salem, S. Da'as, O. L. A. Al-Jamal, M. Scott, and I. Mustafa, "Biocompatibility and toxicity of novel iron chelator Starch-Deferoxamine (S-DFO) compared to zinc oxide nanoparticles to zebrafish embryo: An oxidative stress based apoptosis, physicochemical and neurological study profile," *Neurotoxicol Teratol*, vol. 72, pp. 29–38, Mar. 2019, doi: 10.1016/J.NTT.2019.01.004.